Comparison of $Py^{\bullet+}/dU^{\bullet-}$ Charge Transfer State Dynamics in 5-(1-pyrenyl)-2′-deoxyuridine Nucleoside Conjugates with Amido-, Ethylenyl-, and Ethynyl Linkers

Samir T. Gaballah,[†,‡] Yasser H. A. Hussein,[†,§] Neil Anderson,[#] Tianquan T. Lian,[#] and Thomas L. Netzel*[,†]

Department of Chemistry, Georgia State University, P. O. Box 4098, Atlanta, Georgia 30302-4098, and Department of Chemistry, Emory University, Atlanta, Georgia 30322

Received: June 21, 2005; In Final Form: September 30, 2005

Femtosecond, picosecond, and nanosecond transient absorbance (TA) and picosecond emission kinetics results are presented for three 5-(1-pyrenyl)-2′-deoxyuridine nucleosides each with a different two-atom linker joining pyrenyl C-1 to uracil C-5. The linkers are respectively −NHCO−, $-(CH_2)_2-$, and −C≡C− for PAdU, PEdU, and PYdU. For all three nucleoside conjugates, most conformers undergo intramolecular charge transfer (CT) from their pyrenyl $^1(\pi,\pi^*)$ excited states to form $Py^{\bullet+}/dU^{\bullet-}$ CT products in ultrashort times: ≤0.6 ps for PAdU, ≤30 ps for PEdU, and ≤100 ps for PYdU (instrumentally limited times). Additionally for all three nucleosides, a small fraction of conformers also undergoes slower intramolecular CT from their pyrenyl $^1(\pi,\pi^*)$ states in times as long as tens of nanoseconds. Importantly, for use of these nucleosides in studies of excess electron transport in DNA, the lifetimes the CT products in MeOH lengthen significantly in the above series: 6.0 ps for PAdU, 560 ps for PEdU (the shortest of three TA lifetime components), and 1.06 ns for PYdU. The effects on pyrenyl−dU nucleoside CT state dynamics due to adding oxygen via both aeration and oxygen saturation are also examined for the PEdU nucleoside in MeOH.

Introduction

Recently, a number of papers have reported spectroscopic and kinetics investigations of the dynamics behavior of photoexcited DNA duplexes and hairpins (HPs) that were substituted with pyrenyl−dU conjugates as a means of learning about the mechanisms of excess electron transport in DNA.[1−5] The combination of lengthened average electron transfer (ET) or charge transfer (CT) lifetime and enhanced CT emission quantum yield in HPs with both a 5-(2-pyren-1-yl-ethylenyl)-2′-deoxyuridine electron source nucleotide (U^{PE}) and 5-XdU trap nucleotides (U^X), where X = Br or F, compared to HPs lacking U^X traps strongly suggested that excess electrons were injected into the DNA stem at pyrimidine sites external to U^{PE} as well via charge separation within U^{PE} itself. Furthermore, the increased CT emission quantum yield in HPs with traps compared to HPs without traps implied that externally injected electrons migrated to uracil in U^{PE} (i.e., $Py^{\bullet+}dU$) and thus indirectly formed the emissive $Py^{\bullet+}/dU^{\bullet-}$ CT state of U^{PE}.[4] Importantly, these conclusions were tested in a second study of DNA duplexes with both a 5-(pyren-1-yl-ethynyl)-2′-deoxyuridine electron source nucleotide (U^{PY}) and a U^F trap nucleotide near U^{PY} but with zero to three intervening, same strand A:T base pairs. As expected because of the rigid ethynyl linker in U^{PY} (compared to the flexible ethylenyl linker in U^{PE}), U^{PY} substituted duplexes did not show enhanced CT emission quantum yields for duplexes with U^F electron traps near U^{PY} compared to duplexes without traps. Furthermore, the average CT lifetime and emission quantum yield of U^{PY} substituted duplexes were independent of U^F trap location. These results strongly suggested that for the most part the excess electron in the $PY^{\bullet+}/dU^{\bullet-}$ CT state of U^{PY} was restrained from hopping to nearby U^F traps due to Coulombic attraction to $PY^{\bullet+}$. Similar absence of charge migration in synthetic DNA hairpins as a result of Coulombic attraction within a contact radical ion pair was reported earlier by Lewis and co-workers.[6]

Of course, conclusions drawn from studies of the dynamics of CT excited states in pyrenyl−dU substituted DNA will always rest on a firmer foundation if companion studies of the dynamics of CT excited states in related and corresponding pyrenyl−dU nucleosides are also available for comparison. Wagenknecht, Fiebig, and co-workers produced DNA duplexes substituted with two kinds of pyrenyl−dU nucleotide conjugates.[2,3,7,8] One type of pyrenyl−nucleotide was based on the 5-(pyren-1-yl)-2′-deoxyuridine (PdU) nucleoside originally prepared and studied by Netzel, Eaton, and co-workers.[9,10] In PdU the pyrenyl and uracil subunits were directly bonded together. The second type of pyrenyl−nucleotide conjugate was based on the PYdU nucleoside (see Figure 1) originally prepared by Korshun and co-workers.[11] The above workers as well as others have examined the photophyical behavior of a number of nucleoside conjugates of pyrene (Py) and 2′-deoxyuridine (dU).[9,12−15] This body of work has established that intramolecular CT is responsible for quenching the emission of the pyrenyl $^1(\pi,\pi^*)$ excited state. The CT product formed is a $Py^{\bullet+}/dU^{\bullet-}$ diradical with a characteristic strong, broad absorbance increase in the 460−590 nm region.[1,9] The $Py^{\bullet+}/dU^{\bullet-}$ CT product emits free of pyrenyl emission in the 465−650 nm region, whereas pyrenyl fluorescence is mixed with CT emission in the 375−465 nm region. Earlier work also reported the transient absorbance (TA) spectrum and kinetics for the 5-(pyren-1-yl-carbonyl)-2′-deoxyuridine (PCOdU) nucleoside with a one-atom carbonyl linker.[9]

* Corresponding author. E-mail: tnetzel@gsu.edu.
† Georgia State University.
‡ Current address: Department of Photochemistry, National Research Center, El Tahrir Street, Dokki, Cairo, Egypt.
§ Current address: P. O. Box 25, Sidi Gaber, 21311, Alexandria, Egypt.
# Emory University.

10.1021/jp053359o CCC: $30.25
Published on Web 11/11/2005

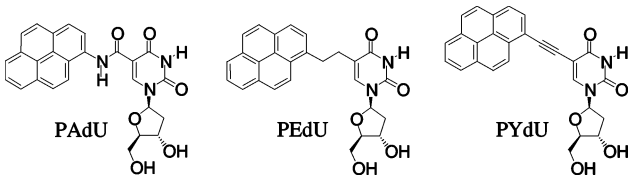

Figure 1. Structural drawings of the PAdU, PEdU, and PYdU pyrenyl−dU nucleoside conjugates with, respectively, amido, ethylenyl, and ethynyl linkers.

For PCOdU in MeOH, the $Py^{\bullet+}/dU^{\bullet-}$ CT product was formed in ≤30 ps and decayed in 67 ps.

Emission lifetime studies of PAdU (see Figure 1) in THF, MeCN, and MeOH showed that CT product emission in the 500−600 nm region decayed with a lifetime of ≤100 ps. Important drawbacks of this previous emission lifetime study were that it could measure neither the actual lifetime of the CT state nor its TA absorbance spectrum. It is worth noting that CIS INDOs (gas phase)[14] and CIS INDOs SCRF (solution phase)[15] computations have been carried out for a model of PAdU, *N*-(1-pyreny)-1-methyluracil-5-carboxamide (PAU_{Me}), to determine the major contributions to the energy variation of CT excited states among pyrenyl−dU nucleoside conformers. In the solution phase, dielectic stabilization was the most important interaction determining of the energy of CT states; in the gas phase, redox and Coulombic effects were most important. To summarize, the dihedral angle between the C5-carbonyl and the uracil plane directly affected two electronic properties of pyrenyl−dU conformers. One was the ease of reduction of the uracil subunit (easier when the CO group was nearly in the uracil plane), and the other was the extent of HOMO and LUMO delocalization onto the atoms that linked the pyrenyl and uracil subunits (more delocalization when the CO group was nearly in the uracil plane). In the gas phase, only the first of these effects was important in determining the energy of CT products, and this effect was modulated by the Coulombic attraction of the cationic and anionic subunits. However, in the solution phase, the extent of HOMO and LUMO delocalization was the dominant determinant of the energy of CT products, because delocalization of these orbitals reduced the dipole moment of their CT products. The CIS INDOs SCRF work showed that lowest energy CT states with sufficiently large dipole moments (≥24 D found in conformers with CO groups out of the uracil plane) had energies below or equal to the energy of the lowest energy pyrenyl $^1(\pi,\pi^*)$ state and that the computed electronic spectrum of *trans*-PAU_{Me} conformers with such lowest energy CT states was similar to that observed for the PAdU nucleoside in MeCN.

This paper reports femtosecond, picosecond, and nanosecond TA and picosecond emission kinetics studies of the formation and decay dynamics for $Py^{\bullet+}/dU^{\bullet-}$ CT products in three pyrenyl−dU nucleosides that differ in the types of linkage used to join their pyrenyl and dU subunits (see Figure 1). All three nucleosides have two-atom linkers, but with varying degrees of free rotation about linking bonds. PYdU with an ethynyl linker (−C≡C−) has only one degree of free rotation between its pyrenyl and uracil subunits, PAdU with a stiff amido linker (−NHCO−) has two degrees of free rotation, and PEdU with an ethylenyl linker ($-(CH_2)_2-$) has three degrees of bond rotation. Combining both new and for PAdU earlier reported emission lifetime and quantum yield results with these TA kinetics results provides a more thorough understanding of the photophysics of intramolecular CT in this series of pyrenyl−dU nucleoside conjugates. The objective of this work is to develop nucleoside conjugates with sufficiently long-lived $Py^{\bullet+}/dU^{\bullet-}$ CT states that they can be used in duplex DNA as the source of an excess electron within the DNA base-stack. Additionally, to lengthen further the lifetime of an excess electron in DNA, previously synthesized *N*,*N*-dimethylanilino-dU (DMAdU) nucleoside conjugates could be combined with pyrenyl−dU conjugates to yield $DMA^{\bullet+}/Py/dU^{\bullet-}$ secondary ET products with potentially longer lifetimes than the primary $Py^{\bullet+}/dU^{\bullet-}$ CT photoproducts.[16] Last, pyridiniumyl−dU electron traps could then be inserted into modified DNA duplexes to provide an optical signal for the arrival of a migrating excess electron at a particular DNA trapping site.[17,18]

Materials and Experimental Methods

General Synthetic Methods. A reference sample and solvents for spectroscopy were purchased from the following vendors and used as received: pyrenebutanoic acid (PBA, high purity grade) from Molecular Probes; methanol (MeOH), acetonitrile (MeCN), and tetrahydrofuran (THF) from Burdick & Jackson (spectroscopic or HPLC grade). Other reagents, chemicals, and solvents were obtained from common suppliers and were usually used without further purification. PAdU was synthesized as described by Kerr et al.;[14] PEdU and PYdU were synthesized as described by Gaballah and Netzel.[19]

UV−Vis Absorbance Spectroscopic Methods. Absorbance spectra were recorded on a Shimadzu UV 2501PC high performance spectrophotometer equipped with a double monochromator for reduced stray light. The spectral bandwidth (SBW) for absorbance spectra was 1 nm, and sample concentrations were $(2-3) \times 10^{-5}$ M. Molar absorbance coefficients (ϵ) of PEdU, PYdU, and PY (1-ethynylpyrene) were measured by weighing 2−3 mg of each compound to ±0.01 mg and dissolving by stirring for 1 week in a 100 mL volumetric flask with the desired solvent. Quantitative dilutions were made to produce Beer's law plots for ϵ calculation. The ϵ values for PEdU were 45.4 mM^{-1} cm^{-1} at 344 nm in THF, 44.6 mM^{-1} cm^{-1} at 343 nm in MeCN, and 45.6 mM^{-1} cm^{-1} at 343 nm in MeOH. See Figure 9 for ϵ values for PYdU and Figure 4S for PY.

UV−Vis Emission Spectroscopy and Emission Quantum Yield Methods. Except where noted otherwise, samples for emission measurements were deoxygenated by bubbling solvent-saturated nitrogen gas into a quartz cuvette equipped with an open-screw cap and a Teflon-silicone septum (Wilmad Glass, Part # WG-9F/OC-Q-10) for 20−30 min while stirring. Emission spectra were recorded on a PTI (Photon Technology International, Inc.) QuantaMaster-1 spectrofluorometer using 5 nm excitation and 2 nm emission SBWs. Spectra were recorded from 350 to 600 nm at 0.5 nm intervals using 2 s integration times at each wavelength. All samples were excited at 341 nm in 1 cm quartz cuvettes using a right-angle excitation and emission geometry. Polarization artifacts were avoided by positioning an achromatic depolarizer in the excitation beam and recording emission spectra through a polarizer adjusted to 54.7° with respect to vertical. All spectra were corrected for the wavelength dependent, emission sensitivity of the fluorometer using appropriate wavelength correction factors (W/cm^2 units) developed at GSU.

For emission quantum yield (Φ_{em}) measurements, reference (r) and unknown (x) solutions were prepared. The absorbances of the reference (PBA in MeOH) and unknown (nucleoside) solutions were matched at 341 nm (A_{341}) to values less than 0.1. All wavelength corrected emission spectra were converted to quanta versus wavelength (quanta corrected) spectra by multiplying the intensity at each wavelength by its corresponding

wavelength value. For the PBA reference solution, the integral of the quanta corrected emission spectrum (D_r) was computed from a direct emission measurement using narrow 1 nm SBWs for both the excitation and emission monochromators. However, the weak emission of the pyrenyl nucleoside solutions prevented using a direct emission method with narrow SBWs. Instead, an indirect procedure reported by Parker and Rees was used.[20,21] This method assumed that the ratio of the emission area to the emission intensity at any convenient wavelength was independent of the excitation intensity and SBW. Thus the integral of the quanta corrected emission spectrum for the unknown hairpin solution (D_x) was measured in two steps. First the ratio of the integral of quanta corrected emission spectrum to emission intensity at a selected wavelength was determined using a broad excitation SBW (5 nm) and a narrow SBW (2 nm) for the emission spectrum plus using the same excitation SBW for an appropriate measurement of the intensity at a convenient wavelength (e.g., broad SBW and a long integration time). Second the emission intensity at the selected convenient wavelength was redetermined with a narrow excitation SBW (1 nm) using the same emission measurement conditions as in the first step. (This procedure matches the narrow SBW excitation condition used for the PBA reference solution and ensures that the absorbances of the reference and unknown solutions are well-defined.) Finally, the product of the ratio defined in the first step times the measured intensity in the second step gives D_x for narrow bandwidth (1 nm) excitation. Emission quantum yields were calculated according to eq 1 with $\Phi_{em}{}^r$ set equal to Φ_{em} for deoxygenated 1-pyrenylbutanoic acid (PBA) in MeOH solution. In turn, the fluorescence quantum yield for PBA (Molecular Probes, Inc., High Purity Grade) in MeOH (spectroscopic or HPLC grade) was itself measured to be 0.065(2)[12] relative to 9,10-diphenylanthracene (Aldrich, 98%) in cyclohexane (spectroscopic or HPLC grade, $\Phi_{em} = 1.00$).[22]

In eq 1, D is the integral of the quanta corrected emission spectra, η is solution refractive index, and A is the absorbance at the excitation wavelength, where r and x subscript refer respectively to reference and unknown samples.[21]

$$\frac{\Phi^x_{em}}{\Phi^r_{em}} = \frac{(D_x \eta_x{}^2/A_x)}{(D_r \eta_r{}^2/A_r)} \qquad (1)$$

Fluorescence Lifetime Methods. All fluorescence decays were recorded on a Tektronix SCD1000 transient digitizer ($\leq$0.35 ns rise time calculated from the bandwidth, $\leq$120 ps rise time for a step input 0.5 times the vertical range) and wavelength resolved with a 0.1 m double monochromator (Instruments SA, Inc. model DH10) in additive dispersion. Two millimeter slits were used, producing an 8 nm band-pass. The 1200 grooves/mm holographic gratings were blazed at 450 nm. After passing through the monochromator, the emission was detected with a Hamamatsu 1564U microchannel plate (200 ps rise time) for short emission lifetimes or a Hamamatsu 928 photomultiplier (2.2 ns rise time) for long ones. The excitation and emission beams were oriented at 90° with respect to each other. Emission was detected through a Glan−Thompson polarizer set at 54.7° ("magic angle") with respect to vertical to eliminate artifacts due to rotational diffusion.[23] Additionally, emission was excited at 355 nm with the third harmonic of an active-passive mode-locked Nd^{3+}/YAG laser manufactured by Continuum, Inc. Typically, 35 μJ excitation pulses of ca. 25 ps duration were collimated into a 3 mm diameter beam and passed through a second Glan−Thompson polarizer set to vertical before entering the sample cuvette. Sample concentrations were adjusted so that the absorbance at 355 nm was 0.13−0.16 in a 1 cm cell, and solution absorbance spectra were measured before and after lifetime measurements to verify that no decomposition occurred during these measurements. PTI, Inc. software was modified by the manufacturer to process up to 1000 data points per decay curve and was used to deconvolute the instrument response from the emission decay to yield exponential lifetime fits to the emission decay data. Typically 10 000 512-point decay curves were averaged. It is important to note that all multi-exponential lifetime fits in this paper have the minimum number of lifetime components that give a good fit (i.e., the kinetics data could not be properly fit with a smaller number of lifetime components). Goodness of fit was judged by minimizing the reduced χ^2 statistic ($\chi_r{}^2$) and producing randomly distributed residuals. The instrument response was obtained by monitoring 355 nm excitation light scattered from an aqueous solution of glycogen. The amount of scattered light was adjusted so that its intensity matched that of the sample's emission decay signal. Reported decay lifetimes (τ_i) are due to least-squares fits of the emission data to interative reconvolutions of three- or four-exponential decay functions (constant term set to zero) and the instrument response function. The sum of the amplitudes (A_i) of the each fit (given in parentheses) is 1.00.

The temporal resolution of the emission kinetics system for multi-exponential emission decays is generally ca. 0.25 ns; however, for nearly single-exponential decays it can be as good as ca. 0.1 ns after deconvolution.[9,10] A full description of the lifetime fitting procedure used here was presented in a recent paper by Netzel et al.[10] Included there are nine sets of emission decays on four time scales (20, 50, 100, and 500 ns) along with the following information: the equations used; plots of residual differences between experimental emission decays and calculated multi-exponential curves; linear and logarithmic plots of emission decays, lamp decays and exponential curves; as well as specific $\chi_r{}^2$ values for the plotted curves.

Femtosecond TA Spectroscopic Methods. The femtosecond tunable visible spectrometer used for this study was based on a regeneratively amplified femtosecond Ti:sapphire laser system from Clark-MXR (1 kHz repetition rate at 800 nm, 100 fs pulse duration (fwhm), 900 μJ/pulse) and nonlinear frequency mixing techniques that have been described previously.[24] The 800 nm output pulse from the regenerative amplifier was split into two parts to generate pump and probe pulses. One part, with 300 μJ/pulse, was frequency doubled and tripled in BBO crystals to generate pump pulses at 800, 400, or 267 nm.

To generate visible probe pulses, about 6 μJ of the 800 nm beam was focused onto a 2 mm thick sapphire window. The intensity of the 800 nm beam was adjusted by setting an iris and inserting ND filters to obtain a stable white light continuum in the 430 nm to beyond the 1000 nm region. Approximately 10 nm spectral bandwidth (SBW) slices of the white light continuum were selected by a variable interference filter (from Optical Coating Laboratory Inc.) to provide tunable probe pulses that were detected by a variable gain photodiode (PDA50 from Thorlabs Inc.). The probe beam passed through an excited region of the sample solution, but every other pump pulse was blocked with a synchronized chopper (New Focus model 3500) at 500 Hz. The TA change was calculated using two adjacent probe−pulse intensities (one for a blocked pump-beam and the other an unblocked pump-beam). About 4% of the chopped pump beam was split by a beam splitter and detected in a second photodiode to monitor the intensity of the pump beam and the phase of the chopper. For each laser firing, the outputs from

the photodiode detectors were integrated in gated boxcar integrators (Stanford Research Systems SR 250), digitized via a 12 bit A-to-D converter (National Instrument AT-MIO-64E-3), and recorded by a PC. Typical peak-to-peak noise in TA measurements was about 0.1−0.2%.

TA spectra at fixed delay times were recorded by scanning the variable interference filter; TA kinetics data at fixed wavelengths were recorded by scanning the delay time. The instrument response was well represented by a Gaussian function with fwhm values ranging from 150 to 300 fs. Thus the instrumental time resolution of the femtosecond TA measurements was 600 fs, and TA kinetics vectors beginning immediately after photoexcitation were fit to exponential functions without convolution of the instrument response. In a typical experiment, a sample of PAdU nucleoside in MeOH was excited at 400 nm with about 2 μJ of pump power, and the subsequent TA was probed by the white light pulses as a functions of time and wavelength. The relative polarizations of the pump and probe beams were set at the magic angle (54.7°) with respect to each other.

Oxygen-free solutions of 0.2 mM PAdU in MeCN and MeOH where prepared by bubbling the stirred the sample solutions for 30 min with boil-off nitrogen gas. These deoxygenated nucleoside solutions were then transferred with the aid of syringes and cannulae in a glovebag under a nitrogen atmosphere to airtight IR cells. The CaF_2 windows of the IR cells were sealed with a slow setting (48 h) extra strength epoxy (ACE number 18611). The glue was applied only to the outer edges of the windows and a 500 μm Teflon spacer kept them separated. The sealed windows in turn were held inside a normal, liquid IR cell mount. Blue, benzophenone ketyl solutions could be kept in freshly glued cells for several days with no absorbance loss. The pump beam's diameter at the sample cell was about 150 μm, and the diameters of the white-light probe beams in the sample cell were about 100 and 200 μm, respectively, for the sample and reference beams. For kinetics data acquisition, a motor continuously translated the whole sample cell at a slow rate. This cell motion prevented photoproducts from accumulating in the photolysis region. TA kinetics measurements were made between 450 and 650 nm for PAdU in both MeCN and MeOH.

Picosecond TA Spectroscopic Methods. The active−passive mode-locked Nd:YAG laser system (1064 nm; 15 Hz repetition rate; ~30 ps pulse duration (fwhm)) at Georgia State University has been described fully in previous reports.[25−27] For this work sample solutions were prepared in air (unless otherwise noted below) to have an absorbance of ca. 0.3 at 355 nm and were excited with circularly polarized third-harmonic pulses from the Nd:YAG laser (~25 ps pulse duration (fwhm) at 355 nm; ~6 mJ/cm^2 per pulse). The monitoring light in the sample and reference beams was depolarized both by scattering from a sand-blazed quartz diffuser disk and by passage through an achromatic depolarizer. In this way possible kinetics artifacts due to photoselection and molecular rotation were eliminated. The excitation beam was ca. 3 mm in diameter for the 1 cm length of the sample cell. The probe beam was ca. 1 mm in diameter and crossed the sample beam inside the sample cell at a small angle, always remaining completely within the photoexcited volume. Fifty to eighty milliliter portions of a stock sample solution were loaded into a sample reservoir and continuously circulated through the sample cell during data acquisition. Aliquots of the sample reservoir solutions were checked during kinetics data acquisition, and whenever more than a few percent loss of initial absorbance was noted, the entire solution in the sample reservoir was changed. Each TA (ΔA) point in a kinetics or spectral plot resulted from averaging data from 960 laser shots (firings), comprising 480 sample photoexcitations and an equal number of blank measurements without sample excitation. The 960 laser shots used for each TA point were taken in alternating groups of 60 shots with excitation and 60 shots without excitation. Finally, TA points in kinetics and spectral experiments were taken in random order.

Nanosecond TA Spectroscopic Methods. To make TA kinetics measurements in the 1 ns to 1 ms time range, samples were excited with a 6 ns duration (fhwm) laser pulse at 341 nm at a 1 Hz repetition rate. The excitation pulse was produced by a Continuum, Inc. Surelite-III-10 Nd:YAG laser system that excited a Contiuum, Inc. ND6000 dye laser. Typically, 425 mJ of frequency doubled output (532 nm) from the Surelite-III-10 yielded 100 mJ of dye laser output at 682 nm. The dye laser output was in turn frequency doubled to 341 nm by a Continuum, Inc. UVT harmonic generator with output tracking feedback control. The Q-switch timing of the Surelite-III-10 was suitably delayed to produce $\leq$3 mJ of excitation energy at 341 nm. The maximum output energy of the combined laser system at 341 nm was 28 mJ. Approximately 3 mL of a solution of PEdU nucleoside in MeOH was held in 1 cm $\times$ 1 cm static quartz cell for TA measurements. The sample absorbances at 341 nm were adjusted to be 0.30 $\pm$ 0.02 through out this study, ca. 1.0 $\times$ 10^{-4} M for PEdU and 2.0 $\times$ 10^{-4} M for PBA. To avoid photoproduct build up in the photolyzed region, all sample solutions were removed from their fixture and mixed after every tenth laser shot. In fact, only a few percent change in the sample's absorbance spectrum was found after ca. 1000 laser shots.

Nanosecond TA kinetics data were acquired using an Edinburgh Analytical Instruments, Ltd. LP920 Laser Flash Photolysis Spectrometer System with a Hamamatsu R955 photomultiplier tube coupled to a Tektronix, Inc. TDS 3012 digital oscilloscope for kinetics and a gated CCD detector for TA spectra. Typical TA kinetics vectors contained 4000 data points. Lifetime fitting of TA kinetics data and spectral analysis were also done using the software supplied as part of the LP920 system. Short lifetime transients were routinely recorded at a data rate of 0.2 ns/channel. Instrument response functions were recorded by measuring the kinetics of 341 nm excitation light scattered from a cell with pure solvent. TA kinetics data were fit by iterative reconvolution of mono- or biexponential functions with the instrument response function and least-squares minimization of the resulting differences between the kinetics data and the convoluted curves. The lifetime resolution limit of this system was 0.5 ns.

Results and Discussion

Femtosecond Spectroscopy of PAdU. Previous spectroscopic investigations of PAdU in deoxygenated THF, MeCN, and MeOH solvents established three main points.[14] One, the initial photoexcited $^1(\pi,\pi^*)$ state of the pyrenyl chromophore is extensively quenched relative to a model pyrenyl compound that cannot undergo intramolecular CT, *N*-acetyl-1-aminopyrene (PAAc): 95% (THF), 96% (MeCN), and 99% MeOH. Additionally, the pyrenyl emission quenching is larger in the more polar solvents (MeCN and MeOH) than in the less polar solvent THF, as expected if the quenching is due to intramolecular CT. Two, the PAdU nucleoside emits from the $Py^{\bullet+}/dU^{\bullet-}$ CT state in all three of the above solvents in the 500−600 nm range to the red of the 370−465 nm emission range for the $^1(\pi,\pi^*)$ state of the pyrenyl chromophore. The red, CT emission is broad

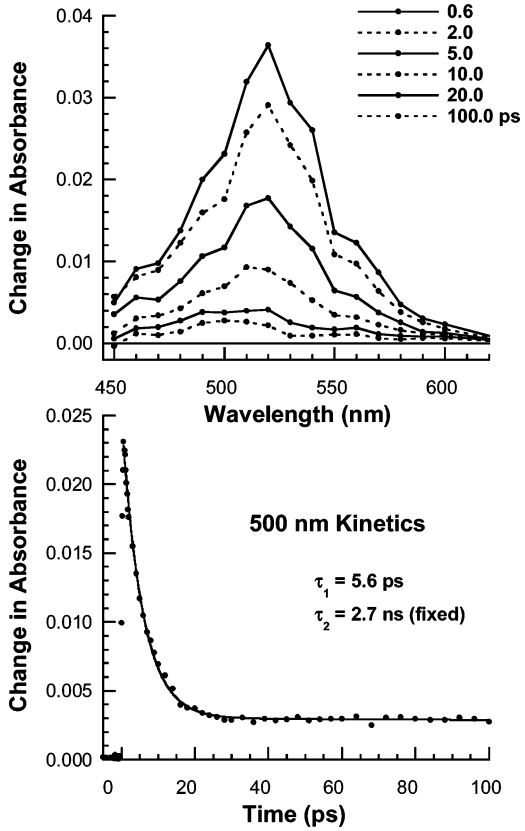

Figure 2. Overlayed femtosecond TA spectral plots from 0.6 to 100.0 ps (top) and a femtosecond TA kinetics plot at 500 nm (bottom) for 1.9×10^{-4} M PAdU in deoxygenaed MeCN. The sample was excited at 400 nm with 100 fs duration (fwhm), 2 μJ pulses in a 500 μm path length cell with CaF_2 windows. The solid curve in the bottom plot is a least-squares fit to the TA data in the 0−1000 ps time range using a biexponential function with a constant term equal to zero and the lifetimes shown in the figure ($R = 0.999$). The average lifetimes (std dev) from TA kinetics fits at 10 wavelengths over the 480−570 nm wavelength range are respectively 5.3 (0.2) ps and 2.7 (1.5) ns for τ_1 and τ_2.

and structureless, whereas emission from the pyrenyl $^1(\pi,\pi^*)$ state shows vibrational structure due to C−C stretching; additionally, the emission lifetime of the ET product is short, ≤100 ps. The third important point is that the pyrenyl emission exhibits up to three apparent decay lifetimes in the ≤100 ps to 25 ns time range. In MeOH, for example, 92−98% of the pyrenyl emission amplitude at 384 and 405 nm has a lifetime of ≤0.3 ns, but up to 8% of it has two decay lifetimes in the 3−5 and 7−23 ns time ranges. In the 500−600 nm region in MeOH, the CT state of PAdU exhibits a single emission lifetime of ≤0.1 ns. In MeCN, the emission kinetics of PAdU in the pyrenyl and CT regions are qualitatively similar to those in MeOH with up to 33% of the pyrenyl emission at 415 and 440 nm decaying with two lifetimes in the 3−5 and 10−13 ns time ranges. The multiexponential emission decay of the pyrenyl chromophore in MeOH and MeCN in the 370−465 regions arises from conformational heterogeneity within solutions of the PAdU nucleoside on time scales of 25 ns or less. In particular, the pyrenyl $^1(\pi,\pi^*)$ states of different conformers undergo intramolecular CT to form the $Py^{\bullet+}/dU^{\bullet-}$ CT state with a wide variety of lifetimes spanning ≤100 ps to 25 ns.

Figure 2 presents femtosecond TA spectra (top) and kinetics results (bottom) for PAdU in deoxygenated MeCN. The main result is that the TA spectra seen in the 0.6−20 ps time range have a strong broad absorbance maximum at 520 nm with a weak shoulder at 560 nm. These TA features are similar to, but red-shifted from, the TA spectra reported previously for the $Py^{\bullet+}/dU^{\bullet-}$ CT state of PCOdU in MeOH.[9] The characteristic CT absorbance features for PCOdU in MeOH occur at 460 nm (maximum) and 500−520 nm (shoulder). Also relevant is the TA spectrum reported for PdU in phosphate buffer at 150 ps after excitation.[1] The CT state of PdU shows strong absorbance features that extend from 450 to beyond 750 nm with a very broad maximum at 590 nm. Thus the characteristic CT absorbance maximum for PAdU in MeCN at 520 nm is intermediate between those of PCOdU and PdU. Figure 1S shows that these TA features are also much the same for PAdU in MeOH. Perhaps surprisingly, in view of the triexponental pyrenyl $^1(\pi,\pi^*)$ emission lifetimes discussed above, all evidence of pyrenyl $^1(\pi,\pi^*)$ states is masked in the TA spectra of Figure 2 by the strong CT product absorbance until the CT products back-react with an average lifetime of 5.3 ± 0.2 ps. In the 20 ps to 1 ns time range, slowly quenched pyrenyl $^1(\pi,\pi^*)$ states decay with an apparent lifetime of 2.7 ± 1.5 ns. This later TA relaxation agrees well with pyrenyl $^1(\pi,\pi^*)$ emission lifetimes in the 3−5 ns time range (ca. 25% amplitude) previously found in MeCN.[14] Combining emission quantum yield and lifetime results with these new TA observations, allows us to draw the following overall picture of the photophysical processes of PAdU in MeCN. Approximately 96% of the pyrenyl $^1(\pi,\pi^*)$ states of PAdU are quenched (based on relative emission quantum yields) within 600 fs of photoexcitation to produce the $Py^{\bullet+}/dU^{\bullet-}$ CT state. This CT state then back-reacts to produce apparently exclusively the ground state of PAdU with an average lifetime of 5.3 ps. In parallel with these forward and reverse, intramolecular ET processes characteristic of most PAdU conformers, approximately 4% of the PAdU nucloside conformers in MeCN undergo ET quenching of their $^1(\pi,\pi^*)$ states in the 3−13 ns time range. Presumbly, the back reaction times for these slowly formed CT products are also only ca. 5 ps. Thus in TA kinetics experiments they would not be observed following the decay of the nanosecond-lived $^1(\pi,\pi^*)$ states. Finally, the TA maximum at 500 nm in Figure 2 for PAdU at 100 ps after photoexcitation accords with the known 490 nm TA maximum of the $S_1(\pi,\pi^*)$ state of the pyrenyl chromophore of 7,8,9,10-tetrahydroxytetrahydrobenzo{*a*}pyrene (BPT) in dimethyformamide and aqueous solutions.[28]

TA spectral and kinetics results for PAdU in MeOH (shown in Figures 1S and 2S, respectively) are remarkably similar to those in Figure 2 for PAdU in MeCN. The $Py^{\bullet+}/dU^{\bullet-}$ CT product is again formed within 600 fs of photoexcitation and absorbs maximally from 520 to 540 nm with a shoulder at 580 nm. The CT product decays with an average lifetime of 6.0 ± 1.1 ps, and again a minority of PAdU conformers ET from their pyrenyl $^1(\pi,\pi^*)$ state slowly with an apparent lifetime of 2.5 ± 1.5 ns. This later TA relaxation agrees well with pyrenyl $^1(\pi,\pi^*)$ emission lifetimes in the 3−5 ns time range (1−5% amplitude) previously found in MeOH.[14] The biggest difference in photophysics for PAdU between the MeCN and MeOH solvents is that (based on relative emission quantum yields) approximately 4% of nucleoside conformers in MeCN undergo slow intramolecular ET quenching of their $^1(\pi,\pi^*)$ states in the 3−13 ns time range, whereas in MeOH approximately only 1% of them do so and in the 3−23 ns time range.

UV−Vis Absorbance and Emission Spectra of PEdU. Figure 3 presents plots of the absorbance and emission spectra of PEdU and PBA both in MeOH. (Figure 3S presents similar spectral plots of PEdU in THF and MeCN.) It is striking how similar the absorbances of these two compounds are in the 300−

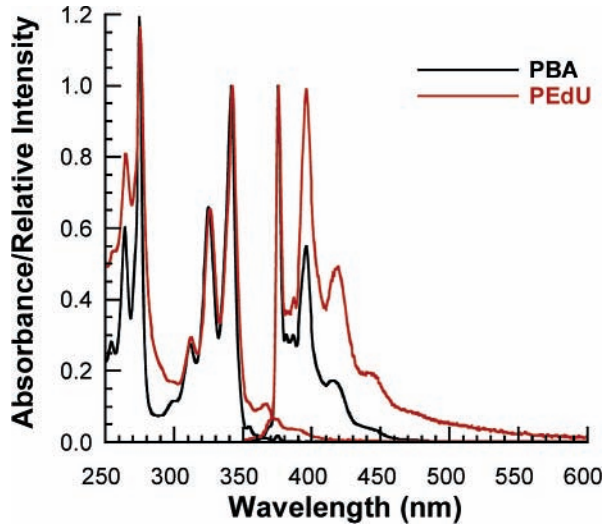

Figure 3. Plots of normalized absorbance and emission spectra for PBA and PEdU in deoxygenated MeOH. The absorbance concentrations were respectively 2.4 and 2.3 × 10^{-5} M for PBA and PEdU in 1 cm path length cells, whereas emission concentrations were respectively 2.9 × 10^{-6} and 2.2 × 10^{-6} M also in 1 cm cells.

TABLE 1: Emission Quantum Yields and Relative Emission Quenching for PBA in MeOH and PEdU in THF, MeCN, and MeOH

compound/ solvent	Φ_{em}^{abs} (%)[a]	Φ_{em}^{rel} (%)[a]	relative quenching (%)[b]
PBA/MeOH	6.5[c]	100	0
PEdU/THF	5.7	88	13
PEdU/MeCN	4.9	75	27
PEdU/MeOH	0.72	11	91

[a] Based on integrating the total emission from 350 to 625 nm. Φ_{em}^{abs} is the absolute emission quantum yield, and Φ_{em}^{rel} is the emission quantum yield relative to PBA in MeOH. [b] A lower limit to pyrenyl $^1(\pi,\pi^*)$ emission quenching relative to PBA in MeOH based on integrating the emission only in the pyrenyl 350−465 nm region. Relative quenching = $(\Phi_{em}^{PBA} - \Phi_{em}^{PEdU})/\Phi_{em}^{PBA}$.

350 nm pyrenyl $S_2(\pi,\pi^*)$ region. Below 300 nm the absorbance of the dU subunit generally causes the absorbance of the nucleoside to exceed that of PBA. Above 350 nm, in the region of the optically forbidden pyrenyl $S_1(\pi,\pi^*)$ state, the nucleoside shows a small amount of increased absorbance over that of PBA. In contrast, although the absorbance of the PEdU nucleoside appears to arise largely from the sum of the absorbances of its two subunits, the emission spectrum of the nucleoside does not look like pure pyrenyl emission. The outstanding difference between the emission spectra for the nucleoside and PBA is that for PBA the emission does not extend beyond 465 nm, whereas for the nucleoside emission extends beyond 600 nm. Red emission in the 500−600 nm region in pyrenyl−dU nucleosides has previously been identified as arising from the $Py^{\bullet+}/dU^{\bullet-}$ CT state.[9,10,13−15] Thus in MeOH PEdU exhibits steady-state emission features from both the lowest energy $^1(\pi,\pi^*)$ state of its pyrenyl subunit and its $Py^{\bullet+}/dU^{\bullet-}$ CT state. Figure 3S shows that the emission spectra of PEdU in THF and MeCN have much less CT contribution than is seen in MeOH.

Emission Quantum Yields of PEdU in THF, MeCN, and MeOH. The dielectric constants (η) of the three solvents studied are 7.6 (THF), 37.5 (MeCN), and 33.6 (MeOH). Table 1 shows that the emission yield of PEdU varies dramatically with change of solvent. The largest emission quenchings occur in the more polar solvents, MeCN and MeOH, compared to emission in the less polar solvent THF. This is understandable, because polar solvents lower the energy of highly polar CT states more than less polar (π,π^*) states. Thus the free energy of CT from the pyrenyl $^1(\pi,\pi^*)$ state is larger in the more polar solvents than in THF.[15] However, the dielectric constants of MeCN and MeOH are not very different, yet there is a large increase of emission quenching in MeOH versus MeCN. This demonstrates that the hydrogen bonding character of MeOH adds substantial stabilization to the $Py^{\bullet+}/dU^{\bullet-}$ CT state in excess of that expected purely from solvent dielectric considerations. For example, a significant hydrogen bonding interaction could reasonably be expected between the hydroxyl group of MeOH and an oxygen atom in the reduced uracil subunit in the CT state. Exactly, the same solvent dependent emission quenching of the pyrenyl $^1(\pi,\pi^*)$ state has been reported previously for the PdU nucleoside in the same solvent series.[9,10] Finally, the significance of hydrogen bonding emission quenching in MeOH compared to MeCN has recently been pointed out in two more studies of PdU.[3,29]

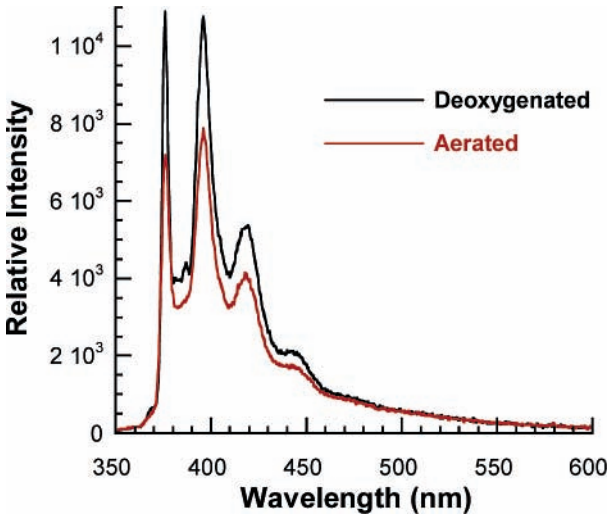

Figure 4. Overlayed plots of emission spectra for 2.2 × 10^{-6} PEdU in MeOH when deoxygenated by bubbling for 40 min with solvent-saturated nitrogen gas and when aerated. Data were recorded on the same sample on the same day; λ_{ex} was 341 nm with 4 nm SBW; emission SBW was 2 nm; 2 s integration time per 0.5 nm data step.

Oxygen Quenching Effects on PEdU Emission Spectra in MeOH. Figure 4 compares the emission spectra of PEdU in deoxygenated and aerated MeOH. The important observation is that the presence of oxygen preferentially lessens emission intensity arising from the pyrenyl $^1(\pi,\pi^*)$ state and within error has no effect on the intensity of emission intensity arising from the CT state (λ_{em} > 465 nm). This result can be understood easily if the emission lifetime of the pyrenyl $^1(\pi,\pi^*)$ state is significantly longer than that of the CT state. The next section discusses PEdU emission lifetimes at various wavelengths in aerated and deoxygentated MeOH and confirms this hypothesis.

Picosecond Emission Kinetics for PEdU in Deoxygenated MeOH. Table 2 presents emission lifetime measurements for PEdU in deoxygenated MeOH at eight wavelengths. The striking result is that in the pyrenyl $^1(\pi,\pi^*)$ emission region from 377 to 450 nm the fits to the emission kinetics data require four exponential decay lifetimes with the longest lifetime component extending to 78 ns. In contrast in the CT region from 500 to 550 nm, three exponential lifetimes are sufficient to fit the data, and the longest lifetime is 11 ns. It is also significant that that the shortest emission lifetime component is 0.5−0.6 ns in the pyrenyl $^1(\pi,\pi^*)$ region and 0.8 ns in the CT region. This shows that the fastest CT state decay lags the fastest pyrenyl $^1(\pi,\pi^*)$

TABLE 2: Picosecond Emission Lifetimes of PEdU in Deoxgenated MeOH[a]

	wavelength (nm)							
	377[b]	396[b]	416[b]	450[b]	475[c]	500[c,d]	525[c,d]	550[c,d]
τ_1 (ns)	0.51	0.61	0.60	0.47	0.55	0.80	0.82	0.78
(A_1)	(0.27)	(0.49)	(0.56)	(0.29)	(0.35)	(0.44)	(0.42)	(0.45)
τ_2 (ns)	5.70	5.18	3.57	1.71	2.62	2.67	2.76	2.63
(A_2)	(0.48)	(0.24)	(0.30)	(0.34)	(0.60)	(0.47)	(0.49)	(0.45)
τ_3 (ns)	10.3	13.8	15.1	3.46	11.0	9.50	10.0	8.59
(A_3)	(0.23)	(0.09)	(0.04)	(0.29)	(0.05)	(0.09)	(0.09)	(0.10)
τ_4 (ns)	78.0	75.5	74.8	77.2				
(A_4)	(0.02)	(0.18)	(0.10)	(0.08)				

[a] λ_{exc} = 355 nm; 25 ps pulse duration (fwhm); PEdU absorbance at 355 nm in a 1 cm path length cell was 0.31. The sample was deaerated by bubbling it with solvent-saturated nitrogen gas while stirring for at least 40 min; 2 mm slits on the ISA DH10 monochromator gave an 8 nm SBW. [b] PMT (Hamamatsu R928) voltage = −700 V; 500 ns digitizer time window. MCP experiments with 50 ns time window showed that there were no ultrafast lifetime components in the 0.1−0.3 ns time range. χ_r^2 values were 0.5, and residuals were ±3.5. [c] MCP (Hamamatsu R1564) voltage = −2300 to −2400 V; 50 ns digitizer time window. Average χ_r^2 values were 5, and average residuals were ±6. [d] Additional experiments with one and two Hoya Y48/+46, Y50/+48, and Y52/+50 glass filters between the sample and the emission detector, respectively, at 500, 525, and 550 nm gave identical kinetics lifetimes showing that the DH10 double monochromator successfully eliminated all pyrenyl emission from these wavelengths. Averaging all nine kinetics measurements in the 500−550 nm region yielded the following average CT-emission lifetime components (amplitudes) with the standard deviation of these components taken as the error of the measurements: 0.76 ± 0.06 ns (0.47), 2.61 ± 0.15 ns (0.44), 9.9 ± 1.2 ns (0.09).

quenching process. In fact the three shortest emission lifetime components in the 377−450 nm region appear to be significantly influenced by the emission decay of the CT state. This point will be examined further when the TA kinetics of PEdU in MeOH are discussed later. The average CT-emission lifetime components (amplitudes) in the 500−550 nm region are 0.76 (0.47), 2.6 (0.44), and 9.9 ns (0.09). See Table 2 for additional details and errors.

Picosecond Emission Kinetics for PEdU in Aerated MeOH. Table 1S presents a summary of emission kinetics measurements for PEdU in aerated MeOH solution. The emission kinetics fall into three categories. In the 377−416 nm region, the kinetics reflect relaxation of the lowest energy pyrenyl $^1(\pi,\pi^*)$ state. In the 500−600 nm region, the kinetics reflect purely relaxation of the $Py^{\bullet+}/dU^{\bullet-}$ CT excited state. In the middle 450−475 nm region, the kinetics have mixed character with some lifetimes characteristic of pyrenyl relaxations and some characteristic of CT state relaxations. Pyrenyl emission decays have longest lifetimes ranging from 7 to 20 ns in aerated MeOH. Consistent with this spectral assignment, the amplitude of the longest emission component progressively decreases from 0.30 to 0.05 over the 377 to 475 nm wavelength range, and in the 500−600 nm range no emission lifetimes are greater than 7 ns. At 377 nm, the emission kinetics can be fit equally well with either three- or four-exponential lifetimes; however, at 416 and 450 nm only four-lifetime fits give randomly distributed residuals. The necessity of using an ultrashort lifetime component (in the 0.1−0.3 ns time range) for pyrenyl $^1(\pi,\pi^*)$ state emission quenching is consistent with TA results discussed below showing that photoexcitation forms the CT state in ≤30 ps. The complicated pyrenyl emission kinetics for PEdU spanning ≤0.1 to 20 ns are a direct consequence of varying intramolecular ET rates within different PEdU nucleoside conformers.

A prominent feature of pyrenyl emission kinetics in Table 1S for PEdU in aerated MeOH is the presence of ultrafast quenching processes in the 0.1−0.3 ns time range. These are absent in Table 2 for PEdU in deoxygenated MeOH. One reason might be that the R928 PMT and the 500 ns time window of the SCD1000 digitizer that were used in the pyrenyl emission region in Table 2 yielded too slow a rise time to follow such fast transients. Indeed this is true. However, we also monitored the pyrenyl emission region in Table 2 using an R1564 MCP detector and a 50 ns time window (the same conditions as in Table 1S). Even with the faster responding MCP detector and a 50 ns time window no TA decays in the 0.1−0.3 ns time range were found for PEdU in deoxygenated MeOH. It cannot be true, however, that ultrafast pyrenyl emission quenching does not occur in this system, because the rise time for CT state formation as seen in TA kinetics is ≤30 ps (see below).

As mentioned above, the pyrenyl emission kinetics for PEdU in deoxygenated MeOH extend to 78 ns, whereas in aerated MeOH the longest emission lifetime is 20 ns. The average emission lifetime at 396 nm for PEdU in deoxygenated MeOH is 16.4 ns, whereas at the same wavelength in aerated MeOH it is 3.2 ns. In contrast, in the CT emission region, the average CT emission lifetime in deoxygenated MeOH is 2.4 ns, whereas in aerated MeOH it is 2.2 ns. Clearly the presence of dioxygen significantly shortens the average pyrenyl $^1(\pi,\pi^*)$ emission lifetime but has a negligible effect on the average CT emission lifetime. This emission kinetics result agrees precisely with the demonstration of differential spectral emission quenching presented in Figure 4. For O_2 to quench pyrenyl $^1(\pi,\pi^*)$ emission in less than 25 ns in aerated MeOH, the quenching reaction must occur within $PEdU{\cdot}O_2$ complexes formed in the ground state prior to photoexcitation. Note that a dioxygen concentration of ca. 10^{-3} M times a bimolecular quenching rate of 10^{10} M^{-1} s^{-1} would yield a diffusional quenching time of 100 ns. Later sections of this paper will discuss additional aspects of static, dioxygen quenching of photoexcited PEdU. However, the CT emission lifetime results in Tables 2 and 1S show that dioxygen does not quench the $Py^{\bullet+}/dU^{\bullet-}$ CT state to an appreciable extent.

Picosecond TA Spectroscopy of PBA and PEdU in MeOH. Figure 5 present plots of TA spectra for PBA and PEdU in aerated MeOH at 25 ps after photoexcitation (top) and of TA kinetics for PEdU at 710 nm (bottom). The presence of dioxygen shortens the lifetime of long-lived pyrenyl $^1(\pi,\pi^*)$ states and thus reduces emission interference from them in the TA measurements. Nevertheless no TA measurements could be made below 460 nm due to emission interferrence in this region for both samples. The TA spectrum of PBA shows an absorbance maximum at 470 nm and a small shoulder at 510 nm. These features agree reasonably with a previously reported absorbance maximum at 490 nm and a broad shoulder in the 510−520 nm region for BPT in dimethyl formamide solution.[28] Similarly, the TA spectrum of pyrene in *n*-octane at 60 ps after excitation has a prominent broad peak at 459 nm, a weaker broad peak at 501 nm, and a weak absorbance band around 560 nm.[30] Only 30% of the initial TA of PBA at 470 nm decays during the 15 ns time window of the picosecond TA experiment (data not shown). This small amount of TA relaxation is consistent with a pyrenyl $^1(\pi,\pi^*)$ singlet lifetime of 20−45 ns assuming, respectively, small to negligible formation of a pyrenyl $^3(\pi,\pi^*)$ state in aerated MeOH (a decay asymptote). For PEdU in aerated MeOH, approximately 70% of the initial TA increase at 470 nm decays during the 15 ns TA time window (data also not shown). This TA decay is consistent with a monoexponential

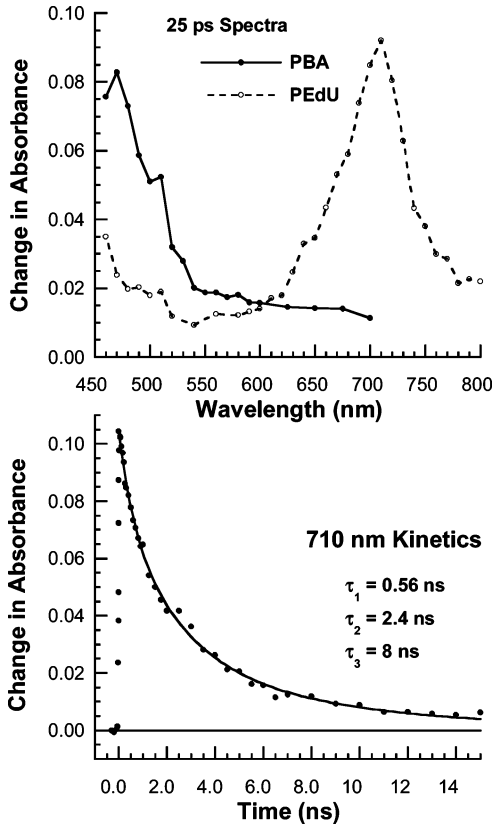

Figure 5. Picosecond TA (ΔA) spectral plots (top) for PBA and PEdU in aerated MeOH at 25 ps after photoexcitation and a picosecond TA kinetics plot (bottom) for PEdU in deoxygenated MeOH at 710 nm: 2.0×10^{-4} M PBA and 1.0×10^{-4} M PEdU. The TA kinetics at 710 nm were fit with a triexponential function without deconvolution of the laser system's instrument response: $\Delta A(t) = m1 \exp(-t/\tau_1) + m2 \exp(-t/\tau_2) + m3 \exp(-t/\tau_3)$. The fit parameters were $m1 = 0.025 \pm 0.013$, $m2 = 0.054 \pm 0.010$, $m3 = 0.025 \pm 0.005$, $\tau_1 = 0.56 \pm 0.24$ ns, $\tau_2 = 2.4 \pm 0.7$ ns, and $\tau_3 = 8 \pm 1.5$ ns. The R value for the fit was 0.998. Fits to a biexponential function also with a constant term equal to zero did not give uniformly distributed residuals.

lifetime of 2.4−9.0 ns assuming, respectively, larger to smaller asymptotes. This range of TA lifetimes agrees with the 2.4−3.7 ns (0.2−0.6 amplitude) emission decay components reported for PEdU in deaerated MeOH in Table 1S. Additionally, the percentage of initial TA signal that decays during the 15 ns time window increases monotonically from 70% to more that 90% as the wavelength increases from 470 to 710 nm. Thus, the shape of the 15 ns TA spectrum of PEdU in MeOH accords generally with the shape of the TA spectrum of the $^1(\pi,\pi^*)$ of PBA. Consequently, part of the TA kinetics of PEdU in aerated MeOH is consistent with relaxation of a pyrenyl $^1(\pi,\pi^*)$ state.

In striking contrast to the TA spectrum of PBA in Figure 5, the TA absorbance spectrum of PEdU also at 25 ps after photoexcitation in aerated MeOH, is entirely different from that of PBA. The prominent features of the TA spectum of PEdU are an absorbance increase at 460 nm and a strikingly strong absorbance maximum at 710 nm. An earlier study by Shafirovich and Geactintov et al.[28] of the BPT cation, formed by two-photon excitation of BPT at 355 nm, shows a narrow pyrenyl cation absorbance ($\epsilon = 3.0 \times 10^4$ M^{-1} cm^{-1}) at 460 nm and weak featureless absorbance beyond 525 nm. Clearly at 25 ps after photoexcitation, PEdU's TA spectrum is not assignable exclusively to the lowest energy pyrenyl $^1(\pi,\pi^*)$ state as it is in PBA. Also, the absorbance decrease from 460 to 540 nm for PEdU is not consistent with the spectrum of the lowest energy pyrenyl $^3(\pi,\pi^*)$ state that absorbs strongly at 420 nm and weakly beyond 440 nm but with a slight absorbance increase from 475 to 525 nm.[28] Thus taken together the 460 nm absorbance increase for PEdU in Figure 5, the strong emission quenching in MeOH for PEdU relative to PBA (>91%) in Table 1, and the red ET product emission in the 500−600 nm region in Figure 4 argue that the TA spectrum at 25 ps after excitation for PEdU in Figure 5 is due to the $Py^{\bullet+}/dU^{\bullet-}$ CT state.

The bottom plot in Figure 5 shows that the TA at 710 nm for PEdU in deoxygenated MeOH has an excitation-pulse-limited rise time (formation in ≤30 ps) and decays with triexponential lifetimes of 0.56 ± 0.24, 2.4 ± 0.7, and 8 ± 1.5 ns. Note that a least-squares fit of the data to a biexponential function, also with a constant term equal to zero, does not give uniformly distributed residuals. Importantly, the fit lifetimes in Figure 5 accord well with the average CT emission lifetimes in dexoxgenated MeOH in Table 1: 0.76 ± 0.06, 2.6 ± 0.15, and 9.9 ± 1.2 ns. Figure 5 shows that the full width at half-maximum (fwhm) of the 710 nm absorbance band of PEdU is ca. 70 nm. Although the case for assigning the 710 nm TA band of PEdU to the $Py^{\bullet+}/dU^{\bullet-}$ CT state at this point is good, it is also worth examining another possible explanation for this band. That is, it could perhaps be due to solvated electrons. In water, solvated electrons have an absorbance maximum at 700 nm ($\epsilon = 1.9 \times 10^4$ M^{-1} cm^{-1}, about two-thirds of that of the pyrenyl cation at 460 nm).[28] However, the fwhm of the 700 nm absorbance band for the solvated electron is well over 200 nm wide (extending from 600 to beyond 800 nm). Additionally, the lifetime of the solvated electron in deoxygenated aqueous solution is ca. 500 ns.[28] Thus the absorbance band at 710 nm for PEdU in MeOH is too narrow, too short-lived, and appears to be too strongly absorbing to be due to solvated electrons. Additional picosecond TA studies of the 710 nm band of PEdU in MeOH are described in the SI material.

Nanosecond TA Spectroscopy of PEdU in Deoxygenated, Aerated, and O_2-Saturated MeOH. Table 3 summarizes the results of a large number of nanosecond TA kinetics measurements of PEdU in MeOH under deoxygenated, aerated, and O_2-saturated conditions. To balance the opposing needs for both detailed and concise results descriptions, only key spectral and kinetics results listed in Table 3 are shown in Figures 6−8. In these studies the samples were excited with 6 ns duration laser pulses at 341 nm. TA rise (or formation) times that were determined by the duration of the excitation pulse are termed "laser limited" in Table 3. As discussed above, both the pyrenyl $^1(\pi,\pi^*)$ and $Py^{\bullet+}/dU^{\bullet-}$ CT states emit. These emissions were detected here as negative TA signals that formed concurrently with photoexcitation, respectively, in the 375−462 and 550 nm regions. As soon as these emissions ceased, positive TA signals due longer-lived excited states and photoproducts were seen in these regions. Just as the rise times of these emission signals were masked by the duration of the excitation pulse, so too their decays masked the rise times of longer-lived states and products with positive TA signals in these regions. Fortunately, the CT emission at 550 nm offered a direct view of the formation and decay times of this important state unobscured by pyrenyl $^1(\pi,\pi^*)$ emission. Basic to understanding PEdU excited state dynamics are (1) the observations above in Tables 2 and 1S that dioxygen does not statically quench the $Py^{\bullet+}/dU^{\bullet-}$ CT state to an appreciable extent and (2) the kinetics data in Table 3 at 550 nm. These latter data show that, independent of the presence or absence of dioxygen (including both aeration and O_2-saturation of MeOH), CT state formation is always excitation-pulse limited, and its decay is always the same within error (ca. 2.5 ns). This result is in excellent agreement with the

TABLE 3: PEdU Nanosecond Photochemistry in MeOH[a]

state	formation time	decay time	λ_{obs} (nm)
	Deoxygenated MeOH		
S_1	laser limited	9.0 ± 1.0 ns	400
		83 ± 3 ns	400
$Py^{\bullet+}/dU^{\bullet-}$	laser limited	3.0 ± 1.2 ns	550
$Py^{\bullet+}$	S_1 decay[b]	>600 ns	462
	Aerated MeOH		
S_1	laser limited	9.0 ± 1.0 ns	420
		3.2 ± 0.5 ns	462
$Py^{\bullet+}/dU^{\bullet-}$	laser limited	2.0 ± 0.5 ns	550
T_1	S_1 decay[b]	156 ± 12 ns	420
		163 ± 7 ns	462
$Py^{\bullet+}$	S_1 decay[b]	>2.5 μs	462
	O_2-Saturated MeOH		
S_1	laser limited	2.2 ± 1.0 ns	375
		3.5 ± 0.5 ns	420
		1.3 ± 0.6 ns	462
$Py^{\bullet+}/dU^{\bullet-}$	laser limited	2.5 ± 1.0 ns	550
T_1	S_1 decay[b]	36 ± 4 ns	420
		36 ± 5 ns	462
$Py^{\bullet+}$	S_1 decay[b]	6.0 ± 0.6 μs	462

[a] Following excitation with a 6 ns duration laser pulse at 341 nm. Conditions: 1 cm path length, static sample cell; 4 mm diameter excitation beam at 90° with respect to the probe beam; 8×10^{-6} M PEdU in MeOH (A_{341} in a 1 cm path length cell was 0.34). The sample solution was deoxygenated in the sample cell by bubbling with solvent-saturated nitrogen gas while stirring for 25−30 min; also the sample solution was oxygen saturated similarly except by bubbling with oxygen gas. Decay and formation times (i.e., lifetimes) were obtained from reconvolution fits of exponential functions to the TA data as described in Figure 6. [b] "S_1 decay" indicates that the absorbance increases (+TA) at 420 nm due to T_1 state formation and at 462 nm due to $Py^{\bullet+}$ (pyrenyl cation) formation were observed as soon as emission (−TA) from the pyrenyl $^1(\pi,\pi^*)$ state ended. Thus, this experiment could not observe T_1 and $Py^{\bullet+}$ formation times that were shorter than the S_1 state's longest decay time in this table. Recall, however, that Table 1 (picoscond emission kinetics) and Figure 5 (picosecond TA kinetics) showed that large fractions of the S_1 state population decayed in subnanosecond times.

dominant average CT emission decay lifetime for PEdU in MeOH in Table 2 (2.6 ns, deoxygenated) and Table 1S (2.4 ns, aerated). Because the lifetimes of the two emitting states have been well discussed above, the remainder of this section focuses on the kinetics of long-lived states (τ > 6 ns) and products that do not emit, namely the pyrenyl $^3(\pi,\pi^*)$ state (T_1) and the pyrenyl cation ($Py^{\bullet+}$).

Figure 6 presents plots of TA spectra at 59 and 347 ns (top) and kinetics at 400 nm (bottom) for PEdU in deoxygenated MeOH. Two observations stand out. First, the TA spectra in the first several hundred nanoseconds are dominated by pyrenyl $^1(\pi,\pi^*)$ emission. The emission kinetics data at 400 nm are well fit with two decay lifetimes of 9 and 83 ns in excellent agreement with 7.5 ns (the amplitude-weighted average of 5 and 14 ns lifetime components) and 76 ns components at 396 nm in Table 2. Second, $Py^{\bullet+}$ absorbance at 463 nm becomes observable after the $^1(\pi,\pi^*)$ emission ends and lasts for >600 ns (see Table 3). Finding the pyrenyl cation present long after the $^1(\pi,\pi^*)$ states have decayed is surprising. Presumably, either the $^1(\pi,\pi^*)$ state or the CT state reduces O_2 that is statically bound to PEdU (even in nitrogen bubbled samples) to form $Py^{\bullet+}$ and $O_2^{\bullet-}$. The long lifetime of the pyrenyl cation would then be due slow charge recombination between these two products. Significantly, as will become clear below, there is no TA absorbance maximum in the 420 nm region in the 347 ns TA spectrum in Figure 6. Such an absorbance maximum would be expected if the pyrenyl T_1 state were formed and lived longer than 100 ns.

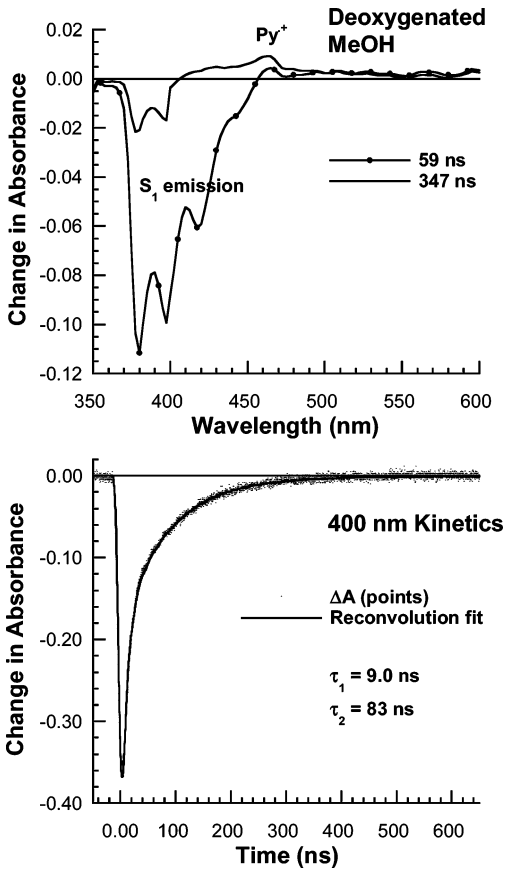

Figure 6. Spectral (top) and kinetics (bottom) plots of nanosecond TA data (ΔA) for 8×10^{-6} M PEdU in deoxygenated MeOH. Experimental conditions are the same as those described in Table 3. In the top plot, the time window for the gated CCD detector was 32 ns and centered at the indicated times after excitation. Each spectrum has 100 data points taken every 2.5 nm and was smoothed over 10 nm wide spectral intervals. In the bottom plot, the negative TA signal (due to pyrenyl S_1 state emission) was recorded at 400 nm with 1.8 nm spectral resolution. The fit lifetimes (amplitude) were $\tau_1 = 9.0 \pm 1.0$ ns (0.21) and $\tau_2 = 83 \pm 3$ ns (0.79), and the constant (asymptote) equaled −0.001.

Figure 7 presents plots of TA spectra at 400 ns (top) and kinetics at 420 nm (bottom) for PEdU in aerated MeOH. One striking new observation in the top spectrum is the presence of TA maxima at 416 and 512 nm. These TA features agree with those expected for the pyrenyl T_1 state. The bottom plot shows that at 420 nm the pyrenyl $^1(\pi,\pi^*)$ emission decays with an apparent lifetime of 9 ns. This also corresponds to the formation time of the T_1 state's TA increase. Eventually, the T_1 state decays with a lifetime of 156 ns. The data in Table 3 for aerated MeOH show that at 462 nm pyrenyl $^1(\pi,\pi^*)$ emission decays with an apparent lifetime of 3 ns, but that the T_1 state's decay lifetime (163 ns) is the same as at 420 nm within error. The different pyrenyl $^1(\pi,\pi^*)$ emission decay lifetimes at 420 and 462 nm agree respectively with 11 ns (the amplitude-weighted average of 4 and 20 ns lifetime components) at 416 nm and 3 ns (the amplitude-weighted average of 2.5 and 9.8 ns components) at 475 nm in Table 1S. Clearly, aerating the MeOH solution of PEdU formed PEdU·O_2 adducts that statically quenched the pyrenyl $^1(\pi,\pi^*)$ state. Some of this $^1(\pi,\pi^*)$ quenching yielded T_1 state products, and some of it also produced $Py^{\bullet+}$ products (and presumably also the corresponding

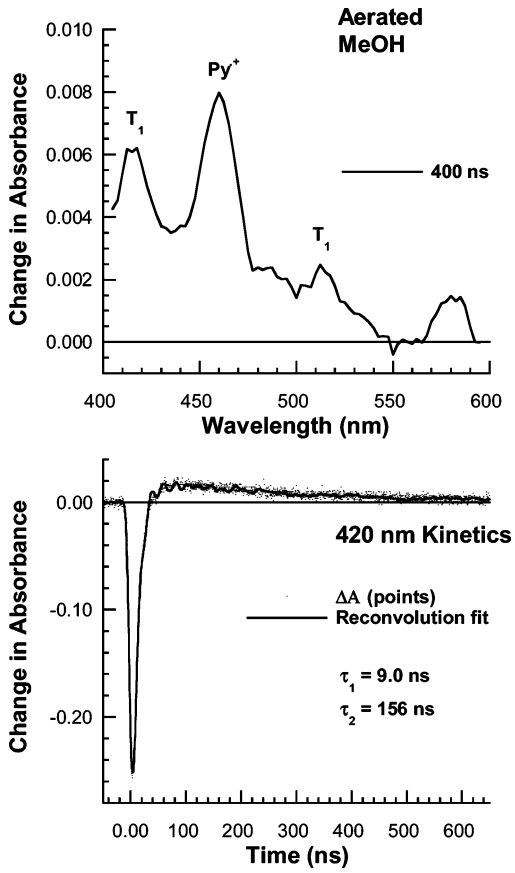

Figure 7. Spectral (top) and kinetics (bottom) plots of nanosecond TA data (ΔA) for 8×10^{-6} M PEdU in aerated MeOH. Experimental conditions were the same as those described in Figure 6 and Table 3. In the top plot, the time window for the gated CCD detector was 200 ns and centered 400 ns after excitation with a 6 ns duration (fwhm) laser pulse at 341 nm. The spectrum has 80 data points taken every 2.5 nm and was smoothed over 10 nm spectral intervals. In the bottom plot, the kinetics data (corresponding to pyrenyl S_1 state emission (−TA) and T_1 state absorbance (+TA)) were recorded at 420 nm with 1.8 nm spectral resolution. The fit lifetimes were $\tau_1 = 9.0 \pm 1.5$ ns and $\tau_2 = 156 \pm 12$ ns, and the constant (asymptote) equaled 0.001.

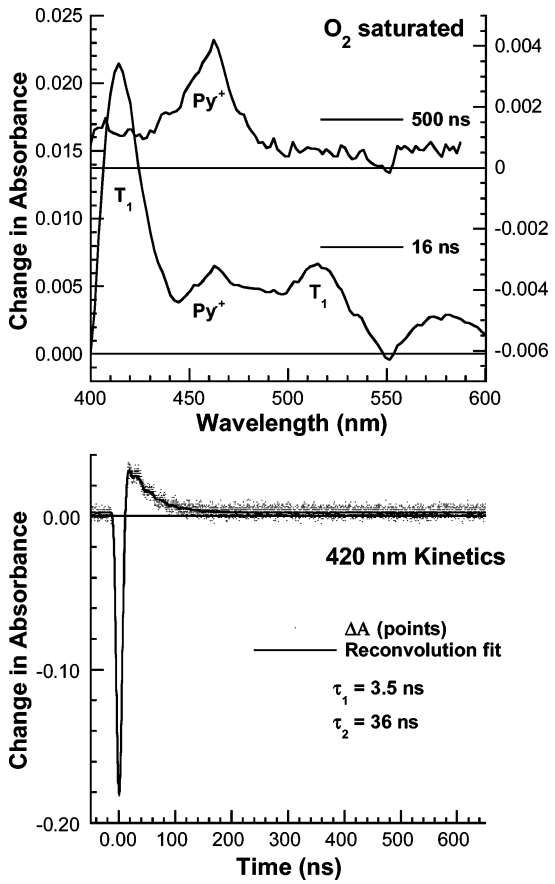

Figure 8. Spectral (top) and kinetics (bottom) plots of nanosecond TA data (ΔA) for 8×10^{-6} M PEdU in oxygen-saturated MeOH. Experimental conditions were the same as those described in Figure 6 and Table 3. In the top plot, the time windows for the gated CCD detector were respectively 200 and 4 ns for the upper and lower traces. The time windows were centered at the indicated times after excitation with a 6 ns duration (fwhm) laser pulse at 341 nm. Each spectrum has 80 points taken every 2.5 nm and was smoothed over 10 nm wide spectral intervals. In the bottom plot, the TA signal (due to pyrenyl S_1 state (−TA) emission and T_1 state absorbance (+TA)) was recorded at 420 nm with 1.8 nm spectral resolution. The fit lifetimes were $\tau_1 = 3.5 \pm 1.0$ ns and $\tau_2 = 36 \pm 4$ ns, and the constant (asymptote) equaled 0.002.

$O_2^{\bullet-}$ products). One clear result was that at 462 nm the TA decreased as the T_1 state decayed (data not shown). If the decay of the T_1 state had yielded $Py^{\bullet+}$ products, the 462 nm absorbance would have increased. It did not; thus only the pyrenyl $^1(\pi,\pi^*)$ and not the $^3(\pi,\pi^*)$ state reacted to form $Py^{\bullet+}$ products. If oxidative quenching of the pyrenyl $^1(\pi,\pi^*)$ state by dioxygen were only mildly exergonic, the competition between formation of the T_1 state and $Py^{\bullet+}$ products would be easy to understand, because it would then be likely that oxidative quenching of the pyrenyl $^3(\pi,\pi^*)$ state would be mildly endergonic and thus too slow to compete with T_1 state decay to the ground state. This, however, is not the case (see below).

Figure 8 presents plots of TA spectra at 16 and 500 ns (top) and kinetics at 420 nm (bottom) for PEdU in O_2-saturated MeOH. The 500 ns spectrum in the plot shows a now familiar 463 nm absorbance due to long-lived (6 μs, see Table 3) pyrenyl cation. The 16 ns spectrum shows, in addition to the 463 nm pyrenyl cation band, T_1 state TA bands at 414 and 514 nm. The strength of the T_1 state's TA absorbance relative to the pyrenyl cation's absorbance at 16 ns in striking. The bottom plot shows that at 420 nm the pyrenyl $^1(\pi,\pi^*)$ emission decays with an apparent lifetime of 3.5 ns, corresponding also to the formation time of the T_1 state's TA increase. Eventually, the T_1 state decays with lifetime of 36 ns. The data in Table 3 for O_2-saturated MeOH show that at 462 nm pyrenyl $^1(\pi,\pi^*)$ emission decays with an apparent lifetime of 1.3 ns and that the T_1 state's decay lifetime (36 ns) is the same as at 420 nm. Comparing pyrenyl $^1(\pi,\pi^*)$ state emission lifetimes for aerated and O_2-saturated MeOH in Table 3, shows that the pyrenyl emission lifetimes at both 420 and 462 nm decreased approximately 3-fold upon O_2 saturation, but under both oxygenation conditions the longer-lived emission was found at the shorter wavelength. Surprisingly, the apparent yield of pyrenyl cation at 500 ns in O_2-saturated MeOH (see Figure 8) was only half of that observed at 400 ns in aerated MeOH (see Figure 7). Thus, increasing the concentration of O_2 that was statically bound to PEdU (i.e., PEdU·O_2 species) increased the rate of intersystem crossing from the pyrenyl $^1(\pi,\pi^*)$ state to the $^3(\pi,\pi^*)$ state but did not similarly increase the rate of oxidative quenching of the pyrenyl $^1(\pi,\pi^*)$ state by dioxygen to form pyrenyl cation (assuming constant cage escape yields for production of solvent separated $Py^{\bullet+}$ and $O_2^{\bullet-}$ products under both aeration and O_2-saturation conditions).

The overall conclusions of the nanosecond TA studies of PEdU in MeOH are that static oxidative quenching of the pyrenyl $^1(\pi,\pi^*)$ state by dioxygen to form small amounts of

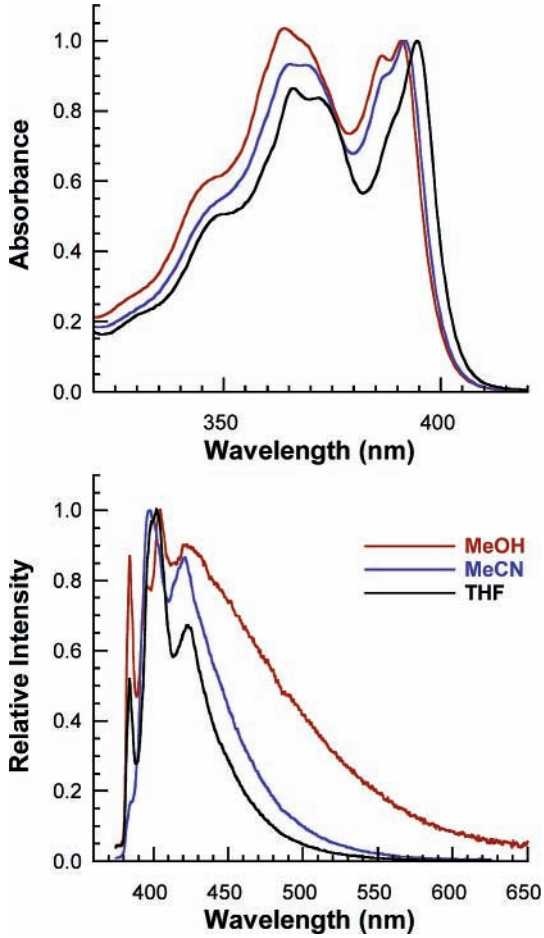

Figure 9. Overlayed plots of absorbance (top) and normalized emission (bottom) spectra for PYdU in the indicated deoxygenated solvents. Absorbance (emission) sample concentrations were respectively 1.9×10^{-5} (8.7×10^{-7}), 2.7×10^{-5} (1.3×10^{-6}), and 4.6×10^{-5} M (3.4×10^{-6} M) in MeOH, MeCN, and THF. Molar absorbances (ϵ) were respectively 53.4 (391), 37.5 (392), and 21.5 $mM^{-1}\ cm^{-1}$ (395 nm) in the same solvent series. The relative emission quantum yields of PYdU were respectively 0.47, 1.5, and 2.1 in deoxygenated MeOH, MeCN, and THF compared to PBA in deoxygenated MeOH.

pyrenyl cation occurs even in solutions of PEdU in MeOH that are deoxygenated by bubbling with nitrogen gas. Surprisingly, aerating the PEdU solutions does not significantly increase the yield of pyrenyl cation but does increase the rate of intersystem crossing from the pyrenyl $^1(\pi,\pi^*)$ to the $^3(\pi,\pi^*)$ state, and T_1 states become observable in TA studies. Finally, saturating the PEdU solution with O_2 actually decreases the yield of pyrenyl cation due to increasing about 3-fold the rate of the pyrenyl $^1(\pi,\pi^*)$ state to $^3(\pi,\pi^*)$ state intersystem crossing apparently without increasing significantly the rate of oxidative quenching of the pyrenyl $^1(\pi,\pi^*)$ state by dioxygen (assuming cage escape yields of $Py^{\bullet+}$ and $O_2^{\bullet-}$ products are independent of the oxygenation state of MeOH). Also, independent of the presence or absence of dioxygen (including both aeration and O_2-saturation of MeOH) CT state formation is remains excitation-pulse limited and its decay lifetime is always the same (ca. 2.5 ns) within error. Last, dioxygen does not oxidatively quench the pyrenyl $^3(\pi,\pi^*)$ state; however, this is not for thermodynamic reasons, as O_2 is easy to reduce ($E_{1/2}(O_2/O_2^{\bullet-} = -0.56$ V (SHE)).[31]

UV−Vis Absorbance and Emission Spectra and Emission Lifetimes for PYdU and PY in MeOH. Figure 9 presents plots of absorbance (top) and emission (bottom) for the PYdU nucleoside in deoyxgenated MeOH, MeCN, and THF. It is not difficult to see in the absorbance spectra that the fine structure of the absorbance band changes as the solvent is varied. In particular, in the $S_1(0,0)$ region (390−400 nm) PYdU in MeOH has two distinct peaks, in MeCN the higher energy peak becomes a shoulder, and in THF this feature is nearly absent. Similar fine structure changes are also present in the emission spectrum. In particular, in MeOH there are clear features at 384, 396 (small shoulder), 404, and 424 nm; in MeCN the previously strong origin peak at 384 is nearly absent and only two peaks at 398 and 423 nm remain with the previous 404 peak in MeOH now only a bulge on the 398 peak; in THF the 384 origin peak is back with clear peaks at 402 and 424 nm with a shoulder at 399 nm. It appears that two sets of correlated emission peaks are present: the very sharp peaks at 384 and 402−404 nm and the broader peaks at 396−398 and 423−424 nm. Figure 4S shows that the principle three peaks (due to C−C vibrations) for 1-ethynylpyrene (PY) are very sharp and occur at 383, 402, and 425 nm in all three solvents. Thus it seems reasonable to assign the sharp two peaks in Figure 9 at 384 and 402−404 nm to "PY-type" features and the two broader peaks at 396−398 and 423−424 nm to "PYdU-type" features.

The interesting question now is are the PY-type features truly due to PYdU nucleoside emission or are they due to PY impurities in the nucleoside sample. The fact that the 384 origin peak varies widely as the solvent is changed for the nucleoside but not at all for PY itself, is a strong internal argument that the PY-type peaks in Figure 9 do indeed arise from the nucleoside and not from PY impurities. Additionally, a second argument supporting this conclusion is that the R_f values of PY and PYdU are very different so that separating them is easy. CHN elemental analysis for PYdU gave measured versus calculated differences, respectively, of 0.07, 0.27, and 0.18%. This agreement is very good but does not necessarily mean that a small amount of PY could not be present in the nucleoside sample. A third argument supporting the above conclusion is that under GC−MS analysis a peak due to PY is easily seen at 290 °C in a sample of PY; in contrast, under the same conditions for a sample of PYdU no PY peak is seen.[32]

For all of the above reasons, it seems clear that the sharp PY-type emission bands in Figure 9 are indeed due to the PYdU nucleoside and not to PY impurities. The broader emission peaks at 400 and ca. 424 nm for PYdU in MeOH were reported earlier, but the sharp PY-type peaks were not seen.[11] Presumably, the spectral resolution (not specified) of the Hitachi MPF-4 spectrofluorometer in the earlier study was set too low to resolve them. Interestingly, the double peak structure in absorbance (Figure 9, top) for PYdU in MeOH in the $S_1(0,0)$ region (390−400 nm) was seen. Also, upon change of solvent to dioxane these two peaks were replaced with a single, red-shifted peak, as is the case here for change of solvent to THF.[33]

Another very important aspect of the emission spectra in Figure 9 (top) not yet mentioned is that they all have broad, structureless emission extending to long wavelengths, and the intensity of their red emission increases in the solvent series THF, MeCN, and MeOH as the solvent type changes from nonpolar, to polar, and finally to polar protic. This red shift of the red emission is exactly what one would except for emission from a $PY^{\bullet+}/dU^{\bullet-}$ CT state. In contrast, the pyrenyl $^1(\pi,\pi^*)$ emission peaks for PY shown in Figure 4S are invariant within this same solvent series. Relatedly, the emission quantum yield of PYdU decreases in the same solvent series (see Figure 9) as pyrenyl $^1(\pi,\pi^*)$ emission is replaced with CT state emission. Table 4 shows that the emission lifetime in the 450−500 nm range for this CT state in MeOH is 1.06 ± 0.02 ns. Thus, PYdU

TABLE 4: Picosecond Emission Lifetimes of PYdU and PY in Deoxygenated MeOH[a]

1.0 PYdU[b]

	wavelength (nm)							
	383	400	425	450	475	500	525	550
τ_1 (ns)	0.13	0.13						
(A_1)	(0.52)	(0.45)						
τ_2 (ns)	1.07	1.04	1.06	1.06	1.06	1.08	1.05	1.06
(A_2)	(0.37)	(0.54)	(1.00)	(1.00)	(1.00)	(1.00)	(1.00)	(1.00)
τ_3 (ns)	38	38						
(A_3)	(0.11)	(0.01)						

2.0 PY[c]

	wavelength (nm)		
	383	403	425
τ_1 (ns)	66	65	65
(A_1)	(1.00)	(1.00)	(1.00)

[a] λ_{exc} = 355 nm; 25 ps pulse duration (fwhm); 2 mm slits on the ISA DH10 monochromator gave an 8 nm SBW; MCP (Hamamatsu R1564) voltage = −2300 to −2550 V. [b] PYdU absorbance at 355 nm in a 1 cm path length cell was 0.32; concentration was 9.7×10^{-6} M. The sample was deoxygenated with five freeze/pump (5×10^{-5} Torr)/thaw cycles on a vacuum line and then loaded into a screw-top sealable cell in a drybox. Twenty nanosecond digitizer time windows were used at all wavelengths, and a 200 ns time window was additionally used at 383 nm. The 38 ns emission decay lifetime found in the 200 ns window was fixed in lifetime fits of data from the 20 ns window at 383 and 400 nm. Average χ_r^2 values were 5.8, and average residuals were ±7.3. [c] PY absorbance at 355 nm in a 1 cm path length cell was 0.18; concentration was 3.0×10^{-6} M. The sample solution was deoxygenated in the sample cell by bubbling with solvent-saturated nitrogen gas for 40 min while stirring. Five hundred nanosecond digitizer time windows were used at all wavelengths, and both PMT (Hamamatsu R920, −700 V) and MCP detectors were used and gave identical lifetimes. Average χ_r^2 values were 3.3, and average residuals were ±6.1.

joins PAdU (τ_{CT} = 6 ps in MeOH) as a pyrenyl−dU nucleoside having a simple, single-exponential CT state lifetime. In contrast, the PEdU nucleoside with a flexible, methylenyl linker exhibits three CT emission decay lifetimes due to the presence of a variety of conformers whose CT states relax at different rates. Another conclusion that the 1.06 ns emission lifetime component for PYdU at all wavelengths in Table 4 and the emission spectra in Figure 9 make clear is that CT emission for PYdU in MeOH extends from 383 to beyond 650 nm, completely overlaping the pyrenyl $^1(\pi,\pi^*)$ emission region. This is an energy range of more than 1.3 eV.

The single, 1.06 ns lifetime of the CT state of PYdU in MeOH contrasts with the wide range of lifetimes of this nucleoside's pyrenyl $^1(\pi,\pi^*)$ state that extend from 0.13 to 38 ns. Presumably, this wide range of pyrenyl emission lifetimes reflects a wide range of intramolecular ET quenching rates among a variety of PYdU conformers. These widely varying intramolecular ET quenching rates likely reflect electronic coupling differences that in turn have their origin in wave function overlap differences between the initial pyrenyl and final CT states of PYdU. In particular, the wave function overlap differences for different PYdU conformers may arise mainly from varying phase relationships among the orbitals of the pyrenyl, ethynyl, and dU subunits of the nucleoside as the relative angle of the pyrenyl and dU planes varies among conformers.

Conclusions

Previously reported pyrenyl emission in the PAdU nucleoside exhibits up to three apparent decay lifetimes in the ≤100 ps to 25 ns time range.[14] In MeOH, for example, 92−98% of the pyrenyl emission amplitude at 384 and 405 nm has a lifetime of ≤0.3 ns, but up to 8% of it has two decay lifetimes in the 3−5 and 7−23 ns time ranges. In the 500−600 nm region in MeOH, the CT state of PAdU exhibits a single emission lifetime of ≤0.1 ns. In MeCN, the emission kinetics of PAdU in the pyrenyl and CT regions are qualitatively similar to those in MeOH. Combining emission quantum yield and lifetime results with these new TA observations, allows us to draw the following overall picture of the photophysical processes of PAdU in MeOH and MeCN. Approximately 96−99% of the pyrenyl $^1(\pi,\pi^*)$ states of PAdU are quenched (based on relative emission quantum yields) within 600 fs of photoexcitation to produce the $Py^{\bullet+}/dU^{\bullet-}$ CT state. This CT state then back-reacts to produce the ground state of PAdU with an average lifetime of ca. 6 ps. Following the 6 ps TA decay due to due to the CT state in both MeOH and MeCN, a second 2−3 ns TA relaxation is seen that agrees well with pyrenyl $^1(\pi,\pi^*)$ emission lifetimes in the 3−5 ns time range. Thus the new TA spectral and kinetics results are in accord with previous emission kinetics experiments and together both support the following model. The multiexponential emission and TA decays of the pyrenyl $^1(\pi,\pi^*)$ state in both MeOH and MeCN arise from conformational heterogeneity within solutions of the PAdU nucleoside on time scales of 25 ns or less. In particular, the pyrenyl $^1(\pi,\pi^*)$ states of different conformers undergo intramolecular ET to form the $Py^{\bullet+}/dU^{\bullet-}$ CT state with a wide variety of lifetimes from ≤600 fs to 23 ns. The CT states of PAdU nucleosides, in contrast, live for only ca. 6 ps in these two solvents.

Table 1 shows that the emission quantum yield of the PEdU nucleoside varies dramatically with a change of solvent. The largest quenchings occur in the more polar solvents, MeCN and MeOH compared to less polar THF. Because polar solvents lower the energy of highly polar CT states more than less polar (π,π^*) states, the free energy of CT from the pyrenyl $^1(\pi,\pi^*)$ state is larger in the more polar solvents than in THF.[15] In accord with this reasoning, intramolecular ET quenching of pyrenyl $^1(\pi,\pi^*)$ emission is therefore also expected to be more efficient in the more polar solvents compared to THF. An important spectral observation for PEdU is that the presence of oxygen preferentially lessens emission intensity arising from the pyrenyl $^1(\pi,\pi^*)$ state and within error has no effect on the emission intensity arising from the CT state (λ > 465 nm). Relatedly, the average emission lifetime at 396 nm for PEdU in deoxygenated MeOH is 16.4 ns, whereas at the same wavelength in aerated MeOH it is 3.2 ns. In contrast in the CT emission region, the average CT emission lifetime in deoxygenated MeOH is 2.4 ns, whereas in aerated MeOH it is 2.2 ns. Clearly the presence of dioxygen significantly shortens the average pyrenyl $^1(\pi,\pi^*)$ emission lifetime but has a negligible effect on the average CT emission lifetime. Thus, the emission kinetics results agree with the observation of differential spectral emission quenching. For O_2 to quench pyrenyl $^1(\pi,\pi^*)$ emission in less than 25 ns in aerated MeOH, the quenching reaction must occur within $PEdU{\cdot}O_2$ complexes formed in the ground state prior to photoexcitation. In the same solution, however, the CT emission lifetime results in Tables 2 and 1S show that dioxygen does not quench the $Py^{\bullet+}/dU^{\bullet-}$ CT state to an appreciable extent.

In contrast to the TA spectrum of PBA in Figure 5, the TA absorbance spectrum of PEdU also at 25 ps after photoexcitation in aerated MeOH, is entirely different from that of PBA. The prominent features of the TA spectum of PEdU are an absorbance increase at 460 nm and a strikingly strong absorbance maximum at 710 nm. Taken together, the 460 nm absorbance increase for PEdU in Figure 5, the strong emission quenching in MeOH for PEdU relative to PBA (>91%) in Table

1, and the red ET product emission in the 500−600 nm region in Figure 4 argue that the TA spectrum at 25 ps after excitation for PEdU in Figure 5 is due to the $Py^{\bullet+}/dU^{\bullet-}$ CT state. The TA of this CT state has an excitation-pulse-limited rise time (formation in ≤30 ps) and decays with triexponential lifetimes of 0.56 ± 0.24, 2.4 ± 0.7, and 8 ± 1.5 ns. Importantly, these TA lifetimes agree well with the average CT emission lifetimes in dexoxgenated MeOH of 0.76 ± 0.06, 2.6 ± 0.15, and 9.9 ± 1.2 ns.

Nanosecond TA data for PEdU show that independent of the presence or absence of dioxygen CT state formation is always excitation-pulse limited, and its decay is always the same within error (ca. 2.5 ns). These results are in excellent agreement with the dominant average CT emission decay lifetimes for PEdU in MeOH noted above. Finding the pyrenyl cation present long after the $^1(\pi,\pi^*)$ states have decayed is surprising. Presumably, the $^1(\pi,\pi^*)$ state reduces O_2 that is statically bound to PEdU (even in nitrogen bubbled samples) to form $Py^{\bullet+}$ and $O_2^{\bullet-}$. The long lifetime of the pyrenyl cation is then due to slow charge recombination between these two products. Aerating the MeOH solution of PEdU forms additional PEdU·O_2 adducts that statically quench the pyrenyl $^1(\pi,\pi^*)$ state. Some of this $^1(\pi,\pi^*)$ quenching yields T_1 state products, and some of it also produces $Py^{\bullet+}$ products (and presumably also the corresponding $O_2^{\bullet-}$ products). Only the pyrenyl $^1(\pi,\pi^*)$ and not the $^3(\pi,\pi^*)$ reacts to form $Py^{\bullet+}$ products. The reaction selectivity of these two excited states is most likely not due to the relative free energies of their reaction channels as both should be very exothermic. Perhaps formation of the $^3(\pi,\pi^*)$ state is accompanied by dissociation of bound O_2. In this case reduction of O_2 by the triplet state would be unlikely due to the slow diffusion of the reactants.

Comparing pyrenyl $^1(\pi,\pi^*)$ state emission lifetimes for aerated and O_2-saturated MeOH in Table 3 shows that the pyrenyl emission lifetimes at both 420 and 462 nm decrease approximately 3-fold upon O_2-saturation. Surprisingly, the apparent yield of pyrenyl cation at 500 ns in O_2-saturated MeOH is only half of that observed at 400 ns in aerated MeOH. Thus, increasing the concentration of O_2 that is statically bound to PEdU increases the rate of intersystem crossing from the pyrenyl $^1(\pi,\pi^*)$ state to the $^3(\pi,\pi^*)$ state but does not similarly increase the rate of oxidative quenching of the pyrenyl $^1(\pi,\pi^*)$ state by dioxygen to form pyrenyl cation (assuming constant cage escape yields for production of solvent separated $Py^{\bullet+}$ and $O_2^{\bullet-}$ products under both aeration and O_2-saturation conditions). Increasing the concentration of O_2 that is statically bound to PEdU does increase the yield and decay lifetime of the pyrenyl $^3(\pi,\pi^*)$ state. This latter state, however, does not form a $^3(Py^{\bullet+}/dU^{\bullet-})$ CT state most likely because this reaction is moderately endothermic.

The rich detail of excited-state relaxations described above can be summarized as shown in Scheme 1. Two populations of PEdU photoexcited nucleosides (S_1) are present, those with O_2 bound (Scheme 1a) and those that are free of O_2 (Scheme 1b), and each decays via different excited-state pathways. For O_2-bound nucleosides, there is competition between charge separation to form $Py^{\bullet+}$ and $O_2^{\bullet-}$ versus intersystem crossing to form the T_1 state and free O_2. For these nucleosides, the CT state is not formed from S_1 as the $Py^{\bullet+}$ and $O_2^{\bullet-}$ photoproducts are lower in energy. Also, the T_1 state does not form the CT state, because the reaction is endergonic. The T_1 state has enough energy to form $Py^{\bullet+}$ and $O_2^{\bullet-}$ products but does not do because diffusion-controlled reactant encounters are infrequent. For nucleosides free of O_2, the S_1 state forms the CT state with a variety of lifetimes depending on the relative conformation of the PEdU subunits, but in most conformers intramolecular CT occurs in ≤30 ps. The CT state relaxes to S_0 without forming the T_1 state indicating that charge recombination is faster than intersystem crossing.

SCHEME 1: Summary of Excited State Relaxations for PEdU in MeOH, Where S_1 Refers to the Pyrenyl $^1(\pi,\pi^*)$ State, T_1 to the Pyrenyl $^3(\pi,\pi^*)$ State, CT to the Charge Transfer State, and S_0 to the Ground State

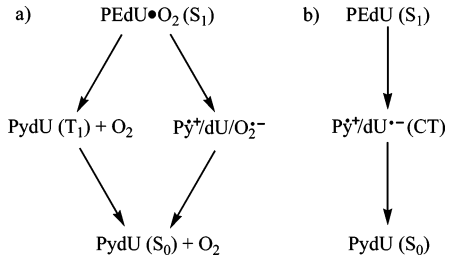

For the PYdU nucleoside, the fine structure of the absorbance band changes as the solvent is varied. In particular, in the S_1-(0,0) region (390−400 nm) PYdU in MeOH has two distinct peaks, in MeCN the higher energy peak becomes a shoulder, and in THF this feature is nearly absent. Similar fine structure changes are also present in the emission spectrum where two sets of correlated emission peaks are present: the very sharp peaks at 384 and 402−404 nm and the broader peaks at 396−398 and 423−424 nm. The sharp two peaks in Figure 9 at 384 and 402−404 nm correspond to "PY-type" features, as are seen in the emission spectrum of PY itself, and the two broader peaks at 396−398 and 423−424 nm arise from "PYdU-type" features unique to the nucleoside.

An important aspect of the emission spectra of PYdU in Figure 9 (top) is that they all have broad, structureless emission extending to long wavelengths, and the intensity of their red emission increases in the solvent series THF, MeCN, and MeOH as solvent type changes from nonpolar, to polar, and finally to polar protic. This red shift of the red emission is exactly what one would except for emission from a $PY^{\bullet+}/dU^{\bullet-}$ CT state. In contrast, the pyrenyl $^1(\pi,\pi^*)$ emission peaks for PY shown in Figure 4S are invariant within this same solvent series. Table 4 shows that the emission lifetime in the 450−500 nm range for this CT state in MeOH is 1.06 ± 0.02 ns. The single, 1.06 ns lifetime of the CT state of PYdU in MeOH contrasts with the wide range of lifetimes of this nucleoside's pyrenyl $^1(\pi,\pi^*)$ state that extend from 0.13 to 38 ns. Presumably, this wide range of pyrenyl emission lifetimes reflects a wide range of intramolecular ET quenching rates among a variety of PYdU conformers. These widely varying intramolecular ET quenching rates likely reflect electronic coupling differences among conformers in the pyrenyl $^1(\pi,\pi^*)$ state. In the CT state of PYdU, however, only a single decay lifetime is seen. Thus PYdU joins PAdU (τ_{CT} = 6 ps in MeOH) as a pyrenyl−dU nucleoside having a simple, single-exponential CT state lifetime. In contrast, the PEdU nucleoside with a flexible, methylenyl linker exhibits three CT emission decay lifetimes.

Acknowledgment. We thank the donors of the Petroleum Research Fund, administered by the American Chemical Society, for support of this research. T.L.N. thanks Marla Netzel for assistance with literature research.

Supporting Information Available: Femtosecond TA spectral and kinetics plots for PAdU in MeCN, absorbance and emission spectra for PEdU in THF and MeCN, picosecond

emission lifetimes for PEdU in aerated MeOH, additional picosecond TA spectroscopic results for PEdU in MeOH, and absorbance and emission spectra for PY in THF, MeCN, and MeOH. This material is available free of charge via the Internet at http://pubs.acs.org.

References and Notes

(1) Kaden, P.; Mayer-Enthart, E.; Trifonov, A.; Fiebig, T.; Wagenknecht, H.-A. *Angew. Chem., Int. Ed.* **2005**, *44*, 1636−1639.

(2) Rist, M.; Amann, N.; Wagenknecht, H.-A. *Eur. J. Org. Chem.* **2003**, 2498−2504.

(3) Amann, N.; Pandurski, E.; Fiebig, T.; Wagenknecht, H.-A. *Chem. Eur. J.* **2002**, *8*, 4877−4883.

(4) Gaballah, S. T.; Vaught, J. D.; Eaton, B. E.; Netzel, T. L. *J. Phys. Chem. B* **2005**, *109*, 5927−5934.

(5) Gaballah, S. T.; Collier, G.; Netzel, T. L. *J. Phys. Chem. B* **2005**, *109*, 12175−12181.

(6) Lewis, F. D.; Liu, X.; Miller, S. E.; Hayes, R. T.; Wasielewski, M. R. *J. Am. Chem. Soc.* **2002**, *124*, 14020−14026.

(7) Wagenknecht, H.-A. *Curr. Org. Chem.* **2004**, *8*, 251−266.

(8) Amann, N.; Pandurski, E.; Fiebig, T.; Wagenknecht, H.-A. *Angew. Chem., Int. Ed.* **2002**, *41*, 2978−2980.

(9) Netzel, T. L.; Nafisi, K.; Headrick, J.; Eaton, B. E. *J. Phys. Chem.* **1995**, *99*, 17948−17955.

(10) Netzel, T. L.; Zhao, M.; Nafisi, K.; Headrick, J.; Sigman, M. S.; Eaton, B. E. *J. Am. Chem. Soc.* **1995**, *117*, 9119−9128.

(11) Korshun, V. A.; Manasova, E. V.; Balakin, K. V.; Prokhorenko, I. A.; Buchatskii, A. G.; Berlin, Y. A. *Russ. J. Bioorg. Chem.* **1996**, *22*, 807−809.

(12) Manoharan, M.; Tivel, K. L.; Zhao, M.; Nafisi, K.; Netzel, T. L. *J. Phys. Chem.* **1995**, *99*, 17461−17472.

(13) Kerr, C. E.; Mitchell, C. D.; Ying, Y.-M.; Eaton, B. E.; Netzel, T. L. *J. Phys. Chem. B* **2000**, *104*, 2166−2175.

(14) Kerr, C. E.; Mitchell, C. D.; Headrick, J.; Eaton, B. E.; Netzel, T. L. *J. Phys. Chem. B* **2000**, *104*, 1637−1650.

(15) Mitchell, C. D.; Netzel, T. L. *J. Phys. Chem. B* **2000**, *104*, 125−136.

(16) Kerr, C. E.; Eaton, B. E.; Netzel, T. L. *Nucleosides, Nucleotides Nucl. Acids* **2000**, *19*, 851−866.

(17) Gaballah, S. T.; Netzel, T. L. *Nucleosides, Nucleotides Nucl. Acids* **2002**, *21*, 681−694.

(18) Gaballah, S. T.; Kerr, C. E.; Eaton, B. E.; Netzel, T. L. *Nucleosides, Nucleotides Nucl. Acids* **2002**, *21*, 547−560.

(19) Gaballah, S. T.; Netzel, T. L. *Heterocycl. Commun.* **2005**, *11*, 241−248.

(20) Parker, C. A.; Rees, W. T. *Analyst (London)* **1960**, *85*, 587−600.

(21) Demas, J. N.; Crosby, G. A. *J. Phys. Chem.* **1971**, *75*, 991−1024.

(22) Berman, H. M.; Young, P. R. *Annu. Rev. Biophys. Bioeng.* **1981**, *10*, 87−114.

(23) Lakowicz, J. R., *Principles of Fluorescence Spectroscopy*; Plenum Press: New York, 1986; p 496.

(24) Ghosh, H. N.; Asbury, J. B.; Weng, Y.; Lian, T. *J. Phys. Chem. B* **1998**, *102*, 10208−10215.

(25) Duncan, D. C.; Netzel, T. L.; Hill, C. L. *Inorg. Chem.* **1995**, *34*, 4640−4646.

(26) Perkins, T. A.; Pourreau, D. B.; Netzel, T. L.; Schanze, K. S. *J. Phys. Chem.* **1989**, *93*, 4511−4522.

(27) Winkler, J.; Netzel, T. L.; Creutz, C.; Sutin, N. *J. Am. Chem. Soc.* **1987**, *109*, 2381−2392.

(28) Shafirovich, V. Y.; Levin, P. P.; Kuzmin, V. A.; Thorgeirsson, T. E.; Kliger, D. S.; Geacintov, N. E. *J. Am. Chem. Soc.* **1994**, *116*, 63−72.

(29) Trifonov, A.; Buchvarov, I.; Wagenknecht, H.-A.; Fiebig, T. *Chem. Phys. Lett.* **2005**, *409*, 277−280.

(30) Foggi, P.; Pettini, L.; Santa, I.; Righini, R.; Califano, S. *J. Phys. Chem.* **1995**, *99*, 7439−7445.

(31) Atkins, P.; de Paula, J. In *Physical Chemistry*; W. H. Freeman and Company: New York, 2002; p 1092.

(32) A final argument supporting the conclusion that the PY-type peaks in Figure 9 arise from the nucleoside itself comes from the emission lifetime measurements for PY and PYdU in MeOH in Table 4. For PY at each of its three principle emission peaks, only a single emission lifetime of 65 ns is seen. In contrast, for PYdU at the 383 and 400 nm PY-type peaks, three emission decay components with average lifetimes (amplitudes) of 0.13 (0.48), 1.06 (0.46), and 38 ns (0.06) are seen. The large-amplitude 0.13 ns ultrafast emission decay in PYdU cannot be due to impurity emission. Similarly, the 38 ns emission component is far from the 65 ns emission lifetime of PY. To check this last point, a 1.04×10^{-5} M solution of PYdU in deoxygenated MeOH was mixed with 3.90×10^{-7} M PY (4% of the PYdU concentration), and the emission decay kinetics were measured at 383 nm with a 500 ns time window that could accurately measure long, but not very short, decay components. Only a single emission decay lifetime of 66 ns was seen. Thus there was no apparent association or interaction of PY with PYdU in the MeOH solution at these concentrations.

(33) In fact there appears to be a labeling error in the earlier paper as the emission spectrum labeled dixonane looks very much like a low resolution version of the emission spectrum of PYdU in MeOH in Figure 9, and similarly the emission spectrum labeled MeOH looks very much like a low resolution version of the emission spectrum of PYdU in THF.